AGU PUBLICATIONS

Tectonics

RESEARCH ARTICLE
10.1002/2016TC004238

Key Points:
- A trench excavation in the epicentral area of the 2012 Emilia earthquake document paleoliquefactions
- Paleoevent timing is constrained based on paleohydrographic analysis, trench log, and C14 ages
- The causative event (Ferrara 1570) is inferred by comparing the macroseismic field

Correspondence to:
R. Caputo,
rcaputo@unife.it

Citation:
Caputo, R., M. E. Poli, L. Minarelli, D. Rapti, S. Sboras, M. Stefani, and A. Zanferrari (2016), Palaeoseismological evidence for the 1570 Ferrara earthquake, Italy, *Tectonics*, *35*, doi:10.1002/2016TC004238.

Received 13 MAY 2016
Accepted 16 MAY 2016
Accepted article online 23 MAY 2016

Palaeoseismological evidence for the 1570 Ferrara earthquake, Italy

R. Caputo[1,2], M. E. Poli[3], L. Minarelli[4], D. Rapti[1], S. Sboras[5], M. Stefani[6], and A. Zanferrari[3]

[1]Department of Physics and Earth Sciences, University of Ferrara, Ferrara, Italy, [2]Research and Teaching Centre for Earthquake Geology, Tyrnavos, Greece, [3]Department of Agricultural, Food, Environmental and Animal Sciences, University of Udine, Udine, Italy, [4]Geotema srl, Ferrara, Ferrara, Italy, [5]NCESD, National Observatory of Athens, Athens, Greece, [6]Department of Architecture, University of Ferrara, Ferrara, Italy

Abstract In May 2012, two earthquakes (M_w 6.1 and 5.9) affected the Po Plain, Italy. The strongest shock produced extensive secondary effects associated with liquefaction phenomena. Few weeks after the earthquakes, an exploratory trench was excavated across a levee of the palaeo-Reno reach, where a system of aligned ground ruptures was observed. The investigated site well preserves the geomorphic expression of a fluvial body that mainly formed in the fifteenth to sixteenth centuries as historical sources and radiometric data testify. In the trench several features pinpointed the occurrence of past liquefaction events: (i) dikes filled with overpressured injected sand and associated with vertical displacements have no correspondence with the fractures mapped at the surface; (ii) thick dikes are buried by the plowed level or even by fluvial deposits; (iii) although some of the 2012 ground fractures characterized by vertical displacement and opening occurred in correspondence of thick dikes observed in the trench, sand and water ejection did not occur; (iv) some seismites (load casts) were observed in the trench well above the 2012 water level. The results strongly suggest that shaking has locally occurred in the past producing a sufficient ground motion capable of triggering liquefaction phenomena prior to, and likely stronger than, the May 2012 earthquake. Historical seismicity documents three seismic events that might have been able to generate liquefaction in the broader investigated area. Based on the analysis of their macroseismic fields, the 17 November 1570 Ferrara earthquake is the most likely causative event of the observed palaeoliquefactions.

1. Introduction

In May 2012, two moderate-to-strong earthquakes, associated with a rich aftershock sequence, affected the eastern sector of the Po Plain, Italy in correspondence of a buried portion of the Northern Apennines (Figure 1a). This fold-and-thrust belt began forming during Late Oligocene due to the collision of a European-provenance continental fragment and the Adria microplate [*Dewey et al*., 1989; *Robertson and Grasso*, 1995; *Mantovani et al*., 1997, 2001]. Since Miocene, the chain has been strongly uplifted and at present it is largely outcropping along central-north Italy. In contrast, the external accretionary wedge is completely buried and masked by the Po Plain deposits as far as the Pliocene-Quaternary sedimentation rate was faster than the rates at which individual blind reverse faults were generating topographic relief [e.g., *Bartolini et al*., 1996; *Maesano and D'Ambrogi*, 2015]. The complete burial of these contractional structures was also favored by the continuous creation of accommodation space due to the overwhelming subsidence of the Adria foreland forced by the double convergence of the Apennines and the Southern Alps [*Castellarin et al*., 1992; *Mariotti and Doglioni*, 2000]. Notwithstanding the "invisible" character of the blind faults underneath the Po Plain [e.g., Burrato *et al*., 2012], their persisting tectonic activity, though characterized by low rates [*Vannoli et al*., 2015; *DISS Working Group*, 2015; *Maesano et al*., 2015], can be inferred from the GPS velocity field of northern Italy showing more than 1 mm/a of N-S convergence [*Devoti et al*., 2011; *Serpelloni et al*., 2015] as well as by seismicity, both historical [e.g., *Guidoboni et al*., 2007; *Rovida et al*., 2011] and instrumental [*Castello et al*., 2006; *Pondrelli et al*., 2006; *Mele et al*., 2007; *Massa et al*., 2012], affecting the broader area (Figure 1b).

In particular, concerning the 2012 events, focal mechanisms [*Pondrelli et al*., 2012; *Cesca et al*., 2013], aftershocks distribution [*Govoni et al*., 2014], differential interferometric synthetic aperture radar analyses [*Bignami et al*., 2012; *Salvi et al*., 2012], and numerical modeling [*Tizzani et al*., 2013] clearly document the reactivation of two roughly E-W trending, south dipping, left-stepping, reverse blind faults. Both structures belong to the central-western sector of the Ferrara Arc, which represents the frontal most expression of the Northern Apennines accretionary wedge [*Pieri and Groppi*, 1981; *Bigi et al*., 1992]. The arc as a whole is

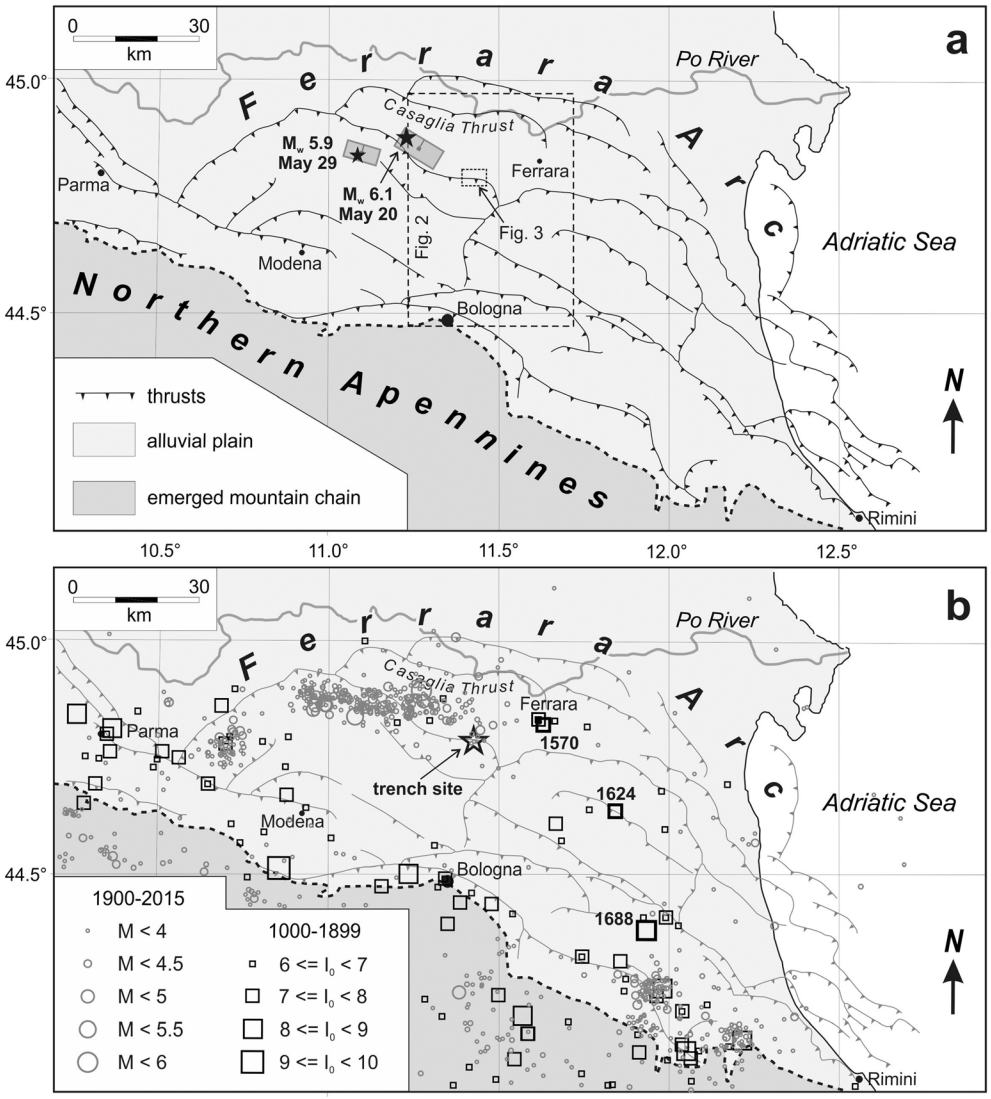

Figure 1. (a) Tectonic sketch map of the Ferrara Arc, Northern Italy, representing the buried frontalmost sector of the Northern Apennines fold-and-thrust belt (modified from *Bigi et al.* [1992]). Stars depict the epicenters of the two main shocks of May 2012 the rectangles the corresponding individual seismogenic sources according to *Database of Individual Seismogenic Sources (DISS) Working Group* [2015]. Location of Figures 2 and 3 are represented by dashed boxes. (b) Seismicity affecting the area in historical (CPTI11) [*Rovida et al.*, 2011] and instrumental times (ISIDe) [*Mele et al.*, 2007]. The historical events of Ferrara 1570 (17 November), Argenta 1624 (18 March), and Romagna 1688 (11 April) are marked by thicker symbols (see Figure 15 for the corresponding macroseismic fields), while the star indicates the trench site.

120–150 km long (Figure 1) and consists of a complex thrust system composed of several interconnected segments, commonly 10–30 km long and characterized by different degrees of overstepping and overlapping geometries [*Pieri and Groppi*, 1981; *Bigi et al.*, 1992; *Boccaletti et al.*, 2004], separated by soft to hard boundary [*Bonini et al.*, 2014]. Faulting along the Ferrara Arc is typically blind. All these tectonic structures are seismogenic and at least capable of producing moderate earthquakes; in case of coseismic linkage with nearby segment(s), the occurrence of strong events could be not ruled out. Two of these segments are the causative faults of the 2012 seismic crisis [*Pezzo et al.*, 2013; *Bonini et al.*, 2014; *Govoni et al.*, 2014; *Vannoli et al.*, 2015].

The Provinces of Ferrara, Modena and Bologna (Emilia Romagna Region), Mantova (Lombardy region), and Rovigo (Veneto Region) were variably affected by the shacking. The first main shock occurred on 20 May at 4:03 A.M. (local time), was the strongest one ($M_L = 5.9$ according to Istituto Nazionale di Geofisica e Vulcanologia and $M_w = 6.1$ according to U.S. Geological Survey), and was followed by several aftershocks (up to $M_L = 5.1$).

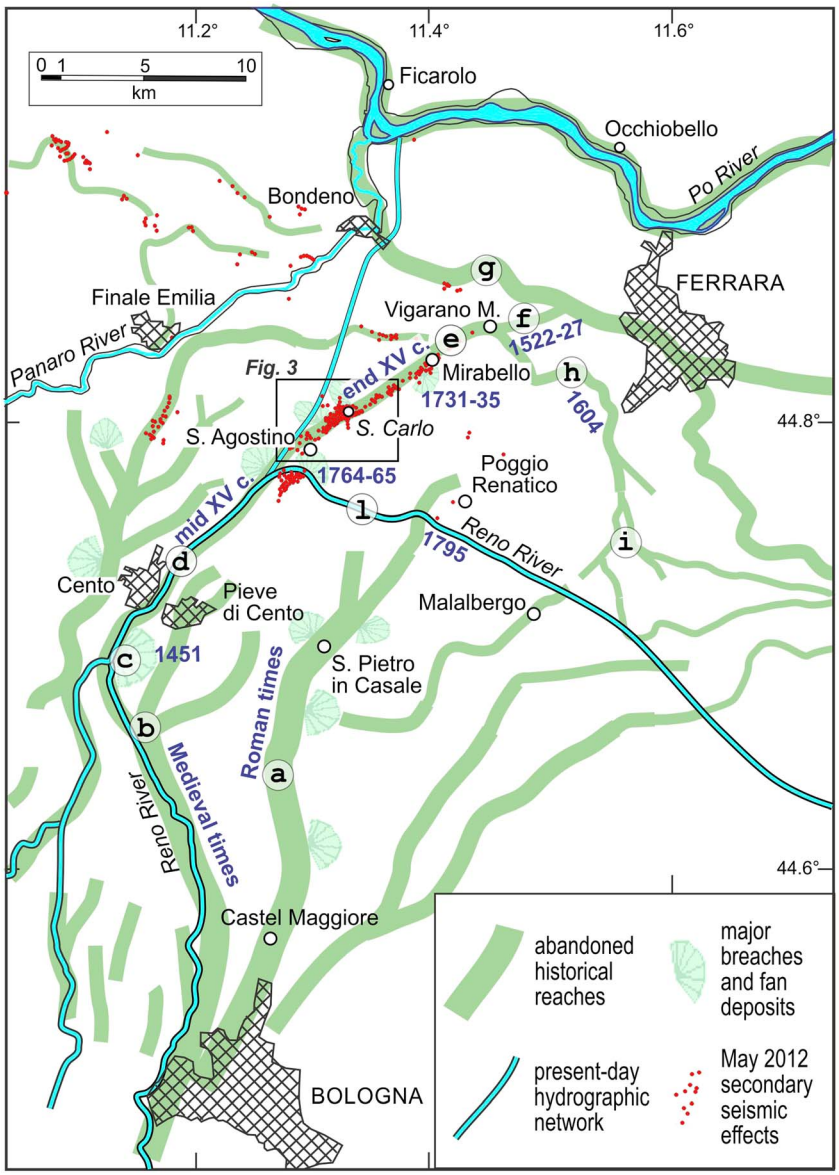

Figure 2. Palaeochannels of the lower Reno River from the mountain exit, southwest of Bologna, toward the Po River and the Adriatic Sea. The line thickness of the abandoned historical reaches is proportional to the channel width. The May 2012 secondary seismic effects include ground ruptures, sand boils and volcanoes, differential settling, and lateral spreading. Labels a to l show relevant hydrographic features; corresponding ages are also indicated (see text for more details). The sixteenth century-to-present road connecting Cento to Ferrara runs along the levee of reaches d, e, and f,.

The first main shock produced numerous secondary geological effects, like ground ruptures, sand boils, and volcanoes, differential settling, and lateral spreading, mainly associated with liquefaction phenomena, which were diffused in the broader epicentral region, particularly along topographic rises and palaeochannels [e.g., *Istituto superiore per la protezione e la ricerca ambientale (ISPRA)*, 2012; *Emergeo Working Group*, 2013] (Figure 2). One cluster of coseismic features affected the area between Sant'Agostino and Mirabello villages, in the southwestern part of the Ferrara Province [e.g., *Papathanassiou et al.*, 2012]. The 29 May event ($M_w = 5.9$) also caused secondary effects, though more limited in intensity and extent, but not in the San Carlo-Sant'Agostino area [*Pizzi and Scisciani*, 2012; *Ninfo et al.*, 2012; *Emergeo Working Group*, 2013; *Rodríguez-Pascua et al.*, 2015]. Similar phenomena also occurred in the past, associated with historical events [e.g., *Galli* 2000; *Papathanassiou et al.*, 2005], including in the eastern Po Plain [*Guidoboni et al.*, 2007].

Due to the widespread diffusion of the coseismic phenomena during the 2012 Emilia earthquake, several papers are available on the topic largely documenting their surface expressions, like ground ruptures, sand boils, volcanic bodies, and linear vents [*Caputo and Papathanassiou*, 2012; *Papathanassiou et al*., 2012; *Di Manna et al*., 2012; *Pizzi and Scisciani*, 2012; *Emergeo Working Group*, 2013; *Chini et al*., 2015]. However, fractures (viz. 2-D features) and dikes (i.e., 3-D bodies) [*Montenat et al*., 2007] could be properly observed and analyzed only through dedicated investigations based on trenching. The main aim of this investigation is to analyze fractures and dikes associated with the 2012 earthquake and possibly documenting the occurrence of palaeoliquefactions, associated with ancient moderate-to-strong seismic events [*Caputo and Helly*, 2008]. To achieve this goal, we applied a typical palaeoseismological approach by excavating an exploratory trench across several ground ruptures formed during the 20 May event.

A novelty of this research is certainly represented by the fact that palaeoseismological trenches are commonly dug across fault traces associated with, and caused by *linear morphogenic earthquakes*, that is to say events that generate a linear morphological feature like a free face [*Caputo*, 2005], and therefore, there is a huge literature on the topic. In contrast, this methodological approach is rarely purposely applied for investigating secondary effects like seismites [*Seilacher*, 1969; *Montenat et al*., 2007]. Although several studies are known for the New Madrid 1811–1812 epicentral area [*Russ*, 1979; *Obermeier*, 1989, 1996; *Saucier*, 1991; *Wesnousky and Leffler*, 1992; *Crone et al*., 1995; *Tuttle and Schweig*, 1995; *Tuttle*, 2001], South Carolina coastal region [*Obermeier et al*., 1987; *Amick et al*., 1990; *Amick and Gelinas*, 1991], Wabash Valley, Central USA [*Munson et al*., 1992, 1994]; California-Oregon marine terraces [*Peterson et al*., 1991], Canada [*Adams*, 1982; *Tuttle*, 1994], NE India [*Sukhija et al*., 1999], Scotland [*Ringrose*, 1989], Turkey [*Hempton and Dewey*, 1983], Venezuela [*Audemard and de Santis*, 1991] and Sweden [*Mörner*, 2003], there are only few cases from northern [*Livio et al*., 2009] and central Italy [*De Martini et al*., 2012]. The present research documents the occurrence of a historical earthquake on a blind thrust, therefore confirming the potential of this investigation technique in similar geological and tectonic contexts.

2. Geological Framework and Quaternary Evolution

The broader alluvial plain of the Po River is fed by sediments drained from both the Apennines and the Alps. The investigated site is located south of the main Po channel and is exclusively fed by water and sediments of Apennines provenance. The outcropping and rapidly rising Northern Apennines mountain chain is dominated by poorly lithified argillaceous melanges, turbiditic successions, and marine claystones. It thus generates a massif terrigenous input to the adjacent alluvial plain. The large sediment availability and the fast foredeep subsidence allowed thick depositional sequences to be rapidly accumulated, throughout Pliocene-Quaternary times [*Bigi et al*., 1992; *Bartolini et al*., 1996]. The very large accumulation rates were globally faster than the tectonically driven creation of accommodation space and consequently the study area progressively evolved from deep marine to continental conditions, during Pleistocene [*Ghielmi et al*., 2010; *Maesano and D'Ambrogi*, 2015].

The fast subsidence has been regionally associated with the bending and roll back of the underthrusting Adria plate likely due to the tectonic load, induced by the progressively growing accretionary wedge [e.g., *Doglioni*, 1993; *Scrocca et al*., 2007]. The buried sector of the Northern Apennines fold-and-thrust belt deforms and partially reactivates structures inherited from the Mesozoic passive continental margin of Adria [e.g., *Rogledi*, 2010; *Di Domenica et al*., 2014; *Bonini et al*., 2014; *Carannante et al*., 2015; *Vannoli et al*., 2015]. The ongoing fault-propagation folding has induced large lateral gradients of syndepositional subsidence, very fast in the synclines, comparatively reduced on the anticline crests [e.g., *Pieri and Groppi*, 1981; *Zoetemeijer et al*., 1992; *Ghielmi et al*., 2010].

The subsidence gradients largely shaped the three-dimensional geometry of the depositional units and significantly affected the fluvial drainage evolution [e.g., *Burrato et al*., 2003]. The fast subsiding areas attracted the fluvial channels and were often the site of large freshwater wetlands, marshes, and shallow lakes; inland fluvial deltas fed by the Apennines rivers frequently prograded into these shallow lakes, also during recent historic times [*Bondesan*, 1989]. In these areas, the sediments accumulated during the last glacial maximum (LGM) are deeply buried, at depth even exceeding 35–40 m [*Stefani and Vincenzi*, 2005; *Molinari et al*., 2007; *Cibin and Segadelli*, 2009]. The hinge areas of the anticlines were instead generally repulsive for the fluvial channel and prone to reworking the older deposits. In these sectors of the plain, condensed sedimentary

successions have hence locally developed. Also, during the May 2012 events fault-propagation folding occurred causing the bending of the topographic surface and the consequent uplift of the broader epicentral area [*Bignami et al*., 2012; *Salvi et al*., 2012; *Caputo et al*., 2015].

The sedimentary unit affected by the liquefaction processes here investigated was deposited into a palaeochannel of the Reno River (Figure 2), which is the largest river outsourced by the Northern Apennines, characterized by a mountain catchment basin area of about 2500 km^2 and dominated by highly erodible lithologies. Before the large impact of engineering works, the Reno River system recorded a high degree of instability (see section 2.2). In the research area, the river sedimentary load is dominated by fine grained sand, silt, and mud content, coarser grained fraction being trapped upstream [*Martelli et al*., 2009]. Indeed, the very low topographic gradients made the sediment transportation difficult and therefore the river channel experienced fast sedimentation and depositional aggradation. The elevated nature of the channels, together with the ongoing tectonic deformation of the area, made river avulsion episodes common [e.g., *Castiglioni et al*., 1999]. The Reno River therefore formed a wide and complex splay of palaeochannels, diverging from a stable outflowing point, few kilometers west of Bologna [*Martelli et al*., 2009] corresponding to the exit site of its valley entrenched in the Apennines hills (Figure 2).

2.1. Shallow Subsurface Statigraphy of the Investigated Area

As a consequence of the above described recent evolution of the Reno River and as it is well documented by subsurface investigations [*ISPRA*, 2009], the uppermost Quaternary stratigraphy of the study area consists of three main units [*Calabrese et al*., 2012]: (i) Upper Pleistocene alluvial plain unit (*PAPU*), (ii) Holocene wetlands unit (*HWU*), and (iii) upper Holocene fluvial channels unit (*FCU*).

The lower unit (PAPU) mainly consists of alluvial plain silt, laterally grading into sand and gravel bodies, deposited into braided river channels. Toward the frontal anticline of the Casaglia thrust, few kilometers to the north of the study site (Figure 1), this stratigraphic unit grades into large volumes of Po River sands. These sediments commonly show well-developed soil horizons, rich in carbonate nodules. The unit was produced by the accumulation of Apennines derived materials, under middle alluvial plain conditions, mainly during the last synglacial phase (latest Pleistocene). The unit never outcrops in the Ferrara Province, and in the study area it is generally buried at the depth of 15–20 m [*Molinari et al*., 2007; *Cibin and Segadelli*, 2009].

The intermediate unit (HWU) is dominated by argillaceous muds, often rich in continental organic matter, grading into freshwater peats. Overbank sand beds are locally developed. The muds accumulated into interfluvial depression wetlands, during part of the Holocene. The unit top is strongly heterochronus and was associated with the development of fluvial channel bodies. In the study area, the unit is 5-to-8 m thick and it is buried at a depth of 7–13 m [*Cibin and Segadelli*, 2009; *Calabrese et al*., 2012].

The upper unit (FCU) is formed by sands accumulated by a Reno River channel(s) during historical times. The unit is 712 m thick and it is capped by the present-day topographic surface. Historical information and radiometric dating (see sections 2.2 and 4.2) suggest that the deposits exposed in the trench and forming the bulk of the levee body at the investigation site was accumulated mainly between the late fifteenth and the early sixteenth century, followed by a rapid fading of the aggradation and a complete halt of the depositional evolution at the beginning of the eighteenth century. The present research is focused on this unit (FCU), that was associated with diffuse, spectacular, and locally severe secondary seismic effects [*Caputo and Papathanassiou*, 2012; *Papathanassiou et al*., 2012; *Di Manna et al*., 2012; *Emergeo Working Group*, 2013], like sand ejection, soil deformation, and lateral spreading phenomena [*Papathanassiou et al*., 2015; *Caputo et al*., 2015].

2.2. Historical Evolution of the Reno River

The stratigraphy above described suggests that no river channel flowed across the investigated site between the latest Pleistocene (LGM) and the late fourteenth century A.D. Through most of the Holocene, the area was dominated by interfluvial plain and marsh environments (HWU). During the Roman period, the Reno was flowing at the east of the study area (*a* in Figure 2), along a channel partly maintained by continuous hydraulic works [*Bondesan*, 2001; *Stefani*, 2006; *Di Cocco*, 2009]. With the demise of the Roman Empire, the interruption of the anthropogenic management and the climate shift toward moister and cooler conditions [e.g., *Enzel et al*., 2003] caused an important reorganization of the drainage network.

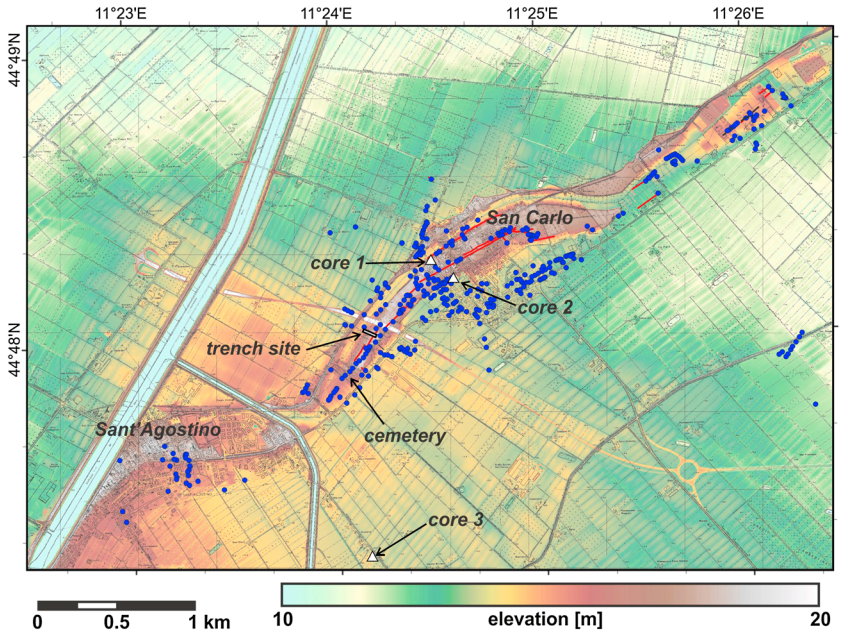

Figure 3. Digital elevation model of the Sant'Agostino-San Carlo area where secondary effects were particularly intense following the 20 May 2012 Emilia earthquake (sand ejection, lateral spreading, ground deformation, differential subsidence, etc.; blue dots). The major ground ruptures are also shown (red lines). Both levees and channel of the historical reach of the Reno River are altimetrically outstanding in the otherwise flat morphology. The investigated trench site and the cores referred to in the text are represented. The high-resolution DEM (5 × 5 m) was provided by Servizio Geologico, Sismico e dei Suoli of Regione Emilia-Romagna.

During early medieval times, the Reno River started to flood large areas [*Cremaschi and Gasperi*, 1989; *Rinaldi*, 2005], at the west of its former Roman Time channel, while from the sixth to the fourteenth century several generations of inland deltas prograded northward, forming a large, diachronous splay of fluvial channel bodies (*b* in Figure 2) [*Cremonini*, 1988, 1991; *Bondesan*, 2001]. In 1451, a major crevasse episode, well documented by historic sources [*Frizzi*, 1848], occurred just upstream of Cento (Rotta della Bisana) and generated a new Reno channel (*c* in Figure 2). The river flooding produced an elongated lake, some meters deep, reaching areas near the town of Ferrara (Vigarano Mainarda; Figure 2). Subsequently, the Reno rapidly developed a new channel body, fast advancing into the elongated lake [*Bondesan*, 2001], with the extraordinary average progradation speed of about 500 m per single autumn-winter interval and with an average sediment thickness of 7–10 m. The new channel was about 150–200 m wide and was flanked by its levees elevated above the surrounding plain (*d* to *e* in Figure 2).

The Reno channel probably reached the trench area during the years 1475–1480, definitely ending there the deposition of the HWU marsh unit and rapidly accumulating most of the FCU channel sands. The fluvial body then rapidly prograded toward the Vigarano Mainarda area, which was reached at about the year 1510 [*Castaldini*, 1989; *Bondesan*, 2001]. In the year 1507, the consecration of the Sant'Agostino parish church on the river levee, 1500 m to the south-southwest of the investigated site, documents that the area was already under subaerial stable conditions.

During the 1522–1527 time interval, an artificial canal was dug (*f* in Figure 2), to force the Reno water to reach the Adriatic Sea, via the southern distributary channels of the Po Delta (*g* in Figure 2) [*Bondesan et al*., 1995]. In the same period, at the investigated site, sediment accumulation on top of the Reno's levee (Figure 3) was so negligible and flooding events so relatively rare to make the tracing of a river-side road (along d, e and f levees, Figure 2), connecting Ferrara to Cento possible.

After an initial success, the artificial inflowing of the Reno into the Po River was soon to encounter growing hydraulic problems, induced by the very low topographic gradient, preventing the fluvial transport of the Reno massive sediment load into the sea. During the year 1604, a large crevasse flooded a widespread area at the southwest of Ferrara and at the east of the study area (*h* in Figure 2). A new generation of inland Reno delta prograded for about 15 km into this freshwater area over one century (*i* in Figure 2). The channel

lengthening and aggradation made the water flux sluggish, forcing the upstream shifting of the crevassing points toward the study site and beyond, with paroxistic flooding at Sant'Agostino, in the period 1731–1735. The Reno water flow in San Carlo was therefore severely reduced, during the eighteenth century, and the remaining channel depression was infilled, producing the uppermost finer grained portion of the study succession (see section 3.2). Further crevasses episodes interrupted the river flow at the investigated site during the fall-winter of the years 1764-1765 [*Fiocca*, 2003]. In the year 1795, the Reno River was eventually forced with massif hydraulic works to reach the sea through the southernmost abandoned distributary channel of the Po (*I* in Figure 2) [*Franceschini*, 1983; *Castaldini and Raimondi*, 1985; *Cazzola et al*., 1995]. Since then, the investigated site remained practically unaltered, with the only exception of some (very) shallow plowing.

3. Palaeoseismological Trench

3.1. Trench Location Selection

In order to directly observe the geometry and distribution at depth of the features induced by the liquefaction phenomena associated with the 2012 earthquakes and to seek possible traces of similar older events, we excavated a trench across the right levee of the palaeo-Reno reach. The trench is located (44°47′57″N, 11°24′05″E) between the cemetery of Sant'Agostino and the village of San Carlo (Figure 3). The investigated site well preserves the geomorphic expression of the sedimentary bodies deposited by the Reno reach during the fifteenth–sixteenth centuries (see section 2.2). The local altitude of the levee, at ~18 m above sea level, is still 4–5 m higher than the surrounding alluvial plain (Figure 3).

The whole relict topographic relief was affected by many ground ruptures, parallel to the channel body elongation (Figures 3 and 4). Immediate postevent surveys document that the ground ruptures at the trench site were several meters long, generally showing a linear geometry in plan view, with a local overlapping and overstepping pattern [*Caputo and Papathanassiou*, 2012, Figure 3c; *Pizzi and Scisciani*, 2012, Figure 2e; *Caputo et al*., 2012, Figure 2]. The prevailing kinematics is characterized by opening (up to 30–35 cm), locally associated with vertical displacement (up to 25–30 cm). At places, ground ruptures characterized by an antithetic kinematics generated small-scale (1–12 m wide) graben structures. Where visible, the observed fracture depth of the gaping fractures was at least 3 m.

All over the grazing area on top of the abandoned levee (Figure 4a) and particularly within the trench perimeter (yellow dashed line), no sand ejection was observed with the exception of few spots, however characterized by limited amounts of outpoured material (Figure 4a). This is testified by direct observations of the authors few hours/days from the event as well as by an aerial survey carried out all over the affected area [see *Bertolini and Fioroni*, 2012, Figure 2b]. This is in striking contrast with the huge amount of ejected sand and water that occurred at only 100–200 m from the trench site as shown in Figures 4c–4f and especially further northeast within the urban area of San Carlo (Figure 3) [e.g., *Caputo and Papathanassiou*, 2012; *ISPRA*, 2012; *Bertolini and Fioroni*, 2012; *Papathanassiou et al*., 2012; *Emergeo Working Group*, 2013], where the geological, morphological, hydrogeological, and stratigraphic settings were quite similar to those at the trench site. This peculiarity and difference, as well as the lack of any building or other major anthropogenic structures in the surroundings, which could produce differential stresses in the subsoil hence influencing the liquefaction process, were the main reasons for the trench site selection. Contrary to other sectors of the levee body, heavily modified by man during the two past centuries, the selected excavation site shows a perfectly preserved depositional morphology lacking any infrastructure that could have altered the subsoil; the only exception being represented by the first half meter of plowed agricultural soil and a shallow water pipeline buried 30 m south of the trench [*Caputo and Papathanassiou*, 2012], which is, however, of no concern for the present discussion.

Prior to trenching, a 115 m long electrical resistivity tomography (ERT; Figure 4a) was acquired, using 1 m spaced electrodes. The geophysical investigation documented the occurrence of mobilized (viz. liquefied) sediments grossly between 5 and 10 m depth [*Abu Zeid et al*., 2012]. This geophysical information contributed to further constraining the trench location.

3.2. Sedimentary Trench Log

The trench was excavated in two stages, during June–July and September 2012. We initially dug a 55 m long and 3-to-5 m wide trench (inset map of Figure 5). For both practical and safety reasons, the excavation

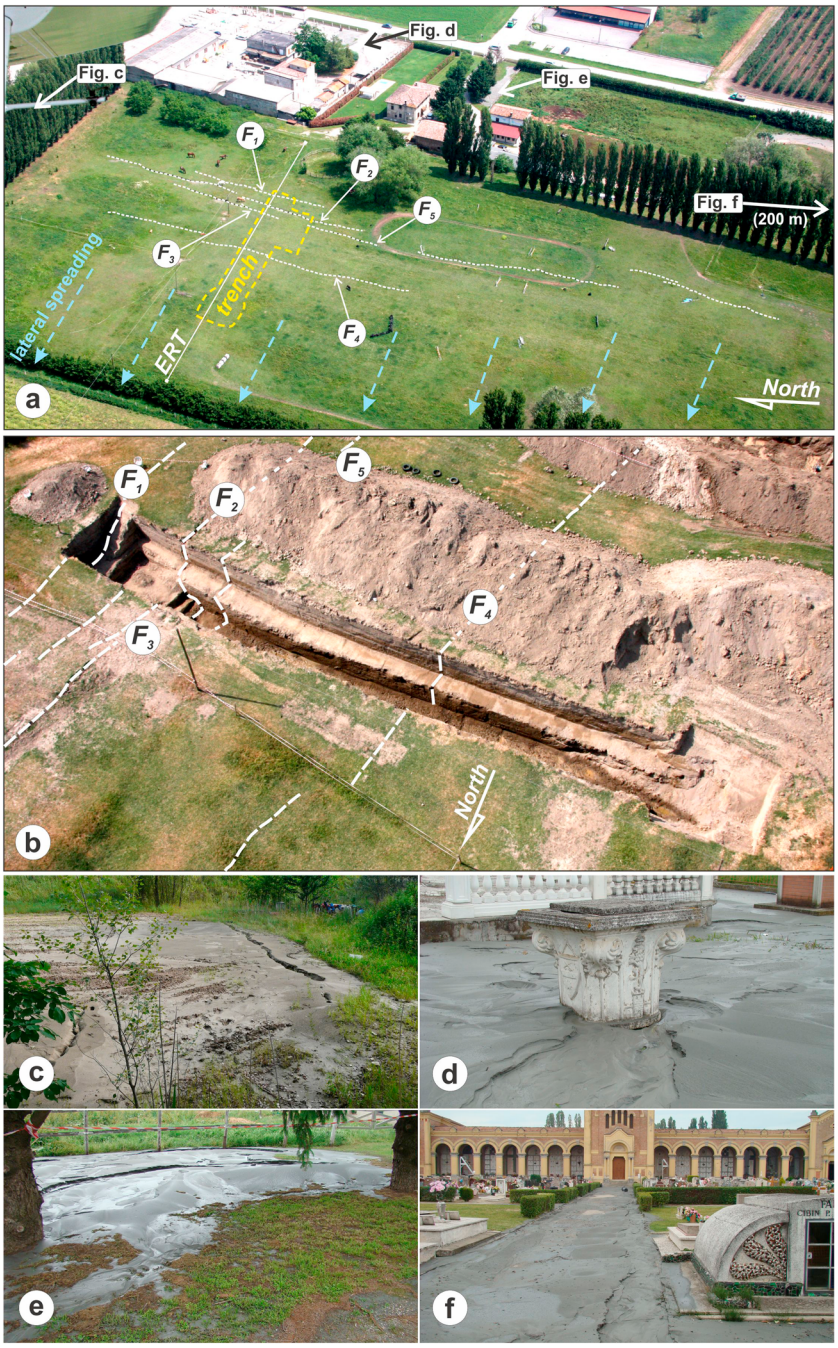

Figure 4. Aerial views of the trench site (a) before and (b) during the excavation operations. Pictures were taken by Giovanni Bertolini (ARPA-RER) on 23 May and 30 June, respectively. In Figure 4a note the high fractures density in the area of the trench (yellow dashed line) which is basically dry (i.e., without sand ejection) and compare with (c–f) nearby sites, where huge amount of water-sand mixture was outpoured at the surface. F1 to F5 label the ground ruptures shown in Figure 5. The arrows indicate the direction of movement associated with the lateral spreading affecting the levee body. The trench site location is indicated in Figure 3. ERT indicates the electrical resistivity tomography published by *Abu Zeid et al.* [2012]. In the upper portion of Figure 4a is visible in the main Ferrara-Cento road referred to in the text.

formed two steps, where only the central one (2 m wide) reached a depth of ~5.5 m from the field surface (Figure 5). The trench was oriented ESE-WNW, i.e., crossing the right levee of the palaeo-Reno River from the morphological top (ESE) toward the abandoned channel depression (WNW; see section 2.2). The very preliminary results of the first excavation phase have been presented in *Caputo et al.* [2012].

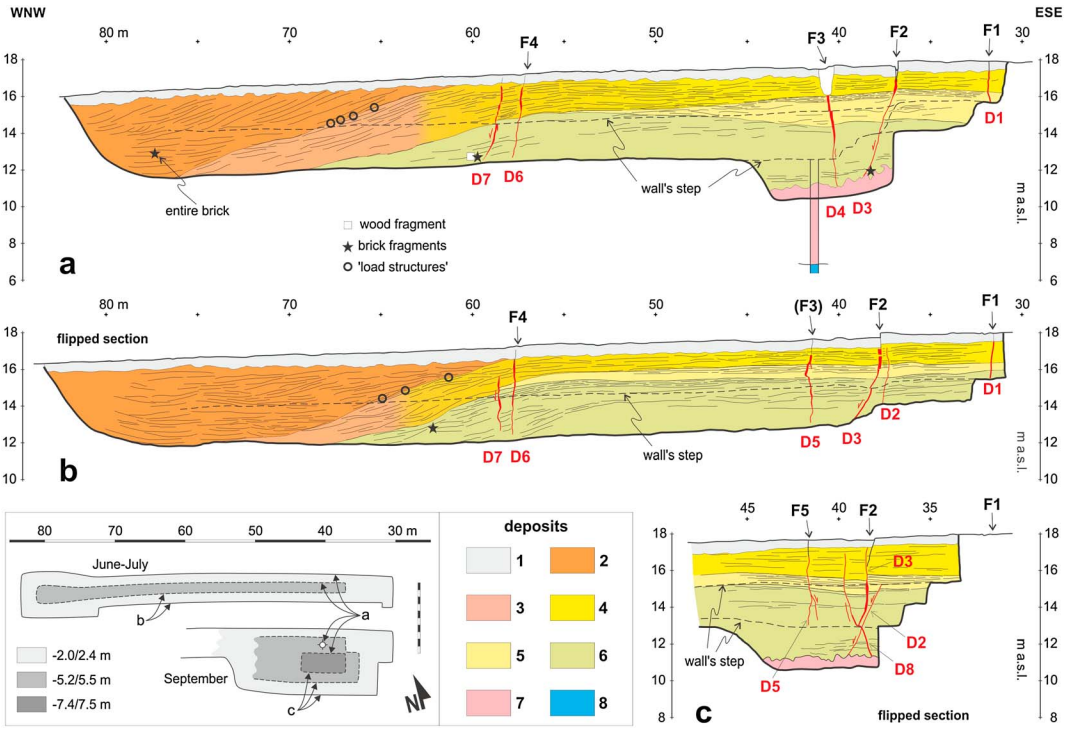

Figure 5. Stratigraphic and structural logs of the trench. Planimetric location of the walls represented in 5a, 6b and 5c is indicated in the inset maps, which also show the two excavation phases of June–July and September 2012; the three gray shades indicate the different excavation depths measured from the topographic surface. The log of the first excavation phase is modified from *Caputo et al.* [2012]. Deposits: (1) plowed layer; (2) medium sands, fluvial channel infilling, and lateral bar; (3) fine sands, lateral bar; (4) sands with minor silt intercalations, natural levee laterally passing to units (3) and (2); (5) fine sands and silts, natural levee older than unit (4); (6) silts and argillaceous silts with minor sandy level, distal natural levee with evidence of plant roots, and some anthropogenic activity; (7) medium-to-coarse gray-to-beige sands, older channel infilling; and (8) clays and silty clays. Deposits (2) to (7) belong to the *Holocene fluvial channels unit* (*FCU*), while deposits (8) belong to the *Holocene wetlands unit* (*HWU*; see section 2.1). The dikes (D#) and the ground ruptures (F#) have been numbered. The location of brick fragments is indicated by black stars, while the wood fragment, sampled for Accelerator Mass Spectrometry dating (Table 1), by a white square.

In a second phase (September), we widened the eastern sector (from m 35 to m 50; inset in Figure 5) up to 10 m in width and then excavated a third step, down to a final trench depth of 7.5 m from the topographic surface. Since the third step was below the piezometric water level, we drilled a 6 m deep borehole starting from the second step (−5.5 m; Figure 5a). The drilling was mainly devoted to create a depression cone by pumping out the water during the excavation and especially the trench logging. However, the borehole was also crucial to extend the observations on the local stratigraphy down to a total depth of ~11 m from the surface (Figure 5a).

The trench investigation provided a good insight on both the fluvial body sedimentary features and deformation structures. The palaeoseismological excavation exposed the channel-levee sand unit (FCU), while the deepest part of the borehole reached the uppermost portion of the underlying clay-rich wetland unit (HWU). Following a detailed logging of the trench walls, two major sedimentological bodies could be recognized.

The majority of the trench section is formed by proximal levee sand and sandy silt intercalations, characterized by direct gradation and tractive lamination structures. The lower portion of the unit witnesses an older channel that was flowing at the southeast of the trench (deposit "6" in Figure 5). This channel was likely formed during the early progradation stages of the late fifteenth century Reno inland delta (see section 2.2). Most of the levee body consists of younger deposits, coeval with the western channel structure still visible today. In the central-eastern sector of the trench, the depositional beds of this younger levee body are subhorizontal and the tractive sedimentary structures record eastward overbank flux directions (deposits "4" and "5").

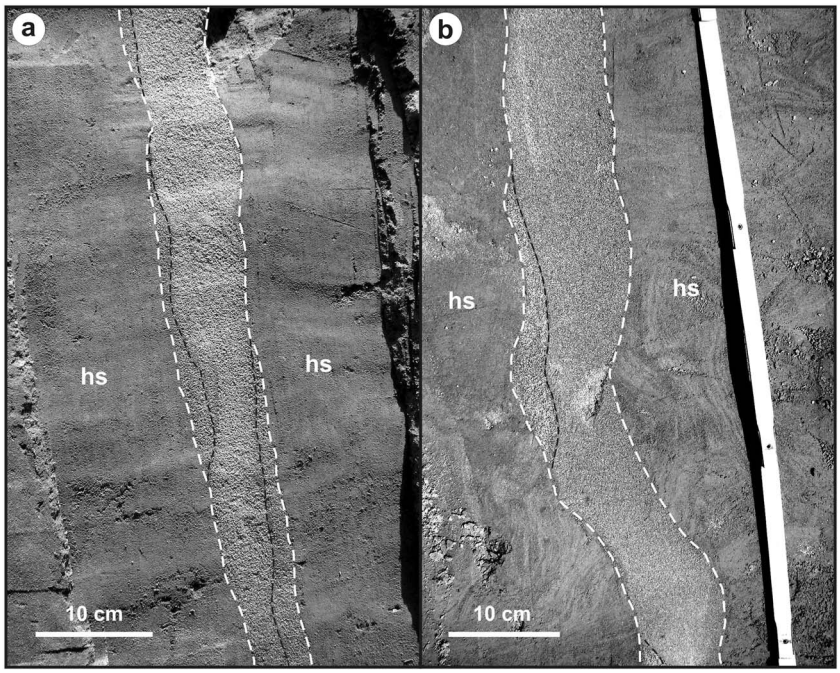

Figure 6. Examples of dikes formed by multiple injections pulses, emphasized by the different grain size and texture of the injected sand. (a) Vertical section across dike D4 at ~3.5 m depth. (b) Horizontal section across dike D4 at ~5 m depth, after the first excavation stage. In both cases, the host sediments (hs) mainly consist of silty sand.

Toward the west, the depositional beds dip westward into the channel sands (up to 15°–20°; deposit "3"), and the contact zone is disturbed by liquefaction, load casts, and compaction structures.

The second sedimentological body outcrops in the western sector of the trench and represents the main channel infilling body (deposit "2" in Figure 5). It mainly consists of medium sand, with a maximum grain diameter of ~1 mm, but it also contains rounded armored mud balls, flat sharp-edged clay intraclasts, wood fragments, freshwater pelecypods and pulmonatae gastropods bioclasts, and brick clasts, sometime of large dimensions. At progressive 77 m (Figure 5a), we found an entire brick, whose dimensions (285 × 140 × 50 mm), proportions and technological features are typical of the late Medieval and Renaissance architecture of the Bologna area [*Gabrielli*, 1999], though brick structures became diffuse along the investigated river channel only during the fourteenth and fifteenth century, being the older buildings mainly wood in structure and more sparse in distribution. The finding of an almost intact brick within the coarse grained sands recording the rapid late infilling phase of this reach of the Reno River (first half of the eighteenth century) suggests a flooding event that involved buildings not far upstream of the trench site, for example, from the Sant'Agostino area (Figure 2).

This sedimentary unit shows well-developed festoon cross stratification and locally contains large fragments of levee silt deposits (up to 2 m wide), "interbedded" within the channel sands. This anomalous setting and lithological mixing are likely associated with sliding phenomena from the river bank. The lower portion of the channel infilling body shows interfingering with the depositional beds of the levee (deposits "3" and "4" in Figure 5). The uppermost fine grained and silty sand was likely deposited during the latest stages of the Reno channel evolution, during the eighteenth century, before the anthopogenic diversion carried out in 1795, few kilometers upstream, at Sant'Agostino (see section 2.2).

3.3. Deformation Features

As above mentioned, the 20 May 2012 main shock triggered diffuse secondary effects, like sand ejection, lateral spreading, ground deformation, and differential subsidence, particularly concentrated in the area between Sant'Agostino and Mirabello (Figure 3). These subsoil phenomena were responsible for most of the superficially observed ground ruptures, including those mapped at the trench site [*Papathanassiou et al.*, 2012, 2015; *ISPRA*, 2012; *Bertolini and Fioroni* 2012; *Emergeo Working Group* 2013; *Caputo and*

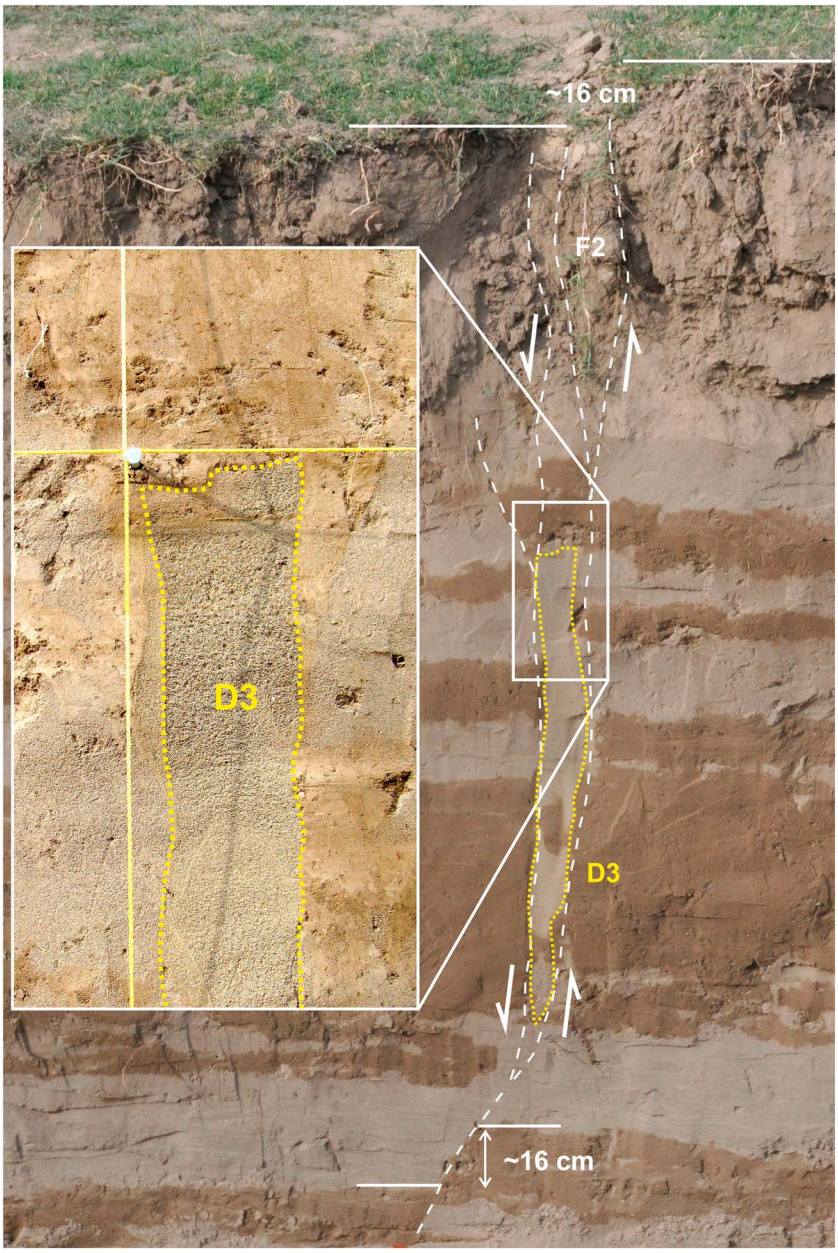

Figure 7. The F2 ground rupture (20 May 2012 earthquake) associated with ~16 cm of throw and 5 cm of heave (i.e., opening at the surface). The fracture at depth used a preexisting dike (D3) as a weakness zone during the lateral spreading sliding. See Figure 5a for location. Notwithstanding the presence of a bent fracture, the 10 cm-wide sand dike (D3) halts at 60 cm depth and it is sealed by the uppermost layers of the levee deposits (modified from *Caputo et al.* [2012]).

Papathanassiou, 2012; *Caputo et al.*, 2015] (Figures 4 and 5). The trench excavation provided a three-dimensional view of some of these coseismic features, confirming the typical geometrical complexities of fracture systems that develop within a mainly extensional stress field, at their early development stage. For example, fractures had rarely a planar shape, commonly showing a variability both in strike and dip angles. The observed kinematics was also similarly complex and laterally variable. Although a shear component was quite common, either strike slip or dip slip, most fractures were associated with some amount of opening.

As expected, all ground ruptures intersected by the excavation (Figure 4a) were also observed in the trench walls as fractures (labeled F# in Figure 5). Some of them could be followed down to the base of the excavation, though their trace in the trench's walls tapers downward, or even disappears, and the displacement

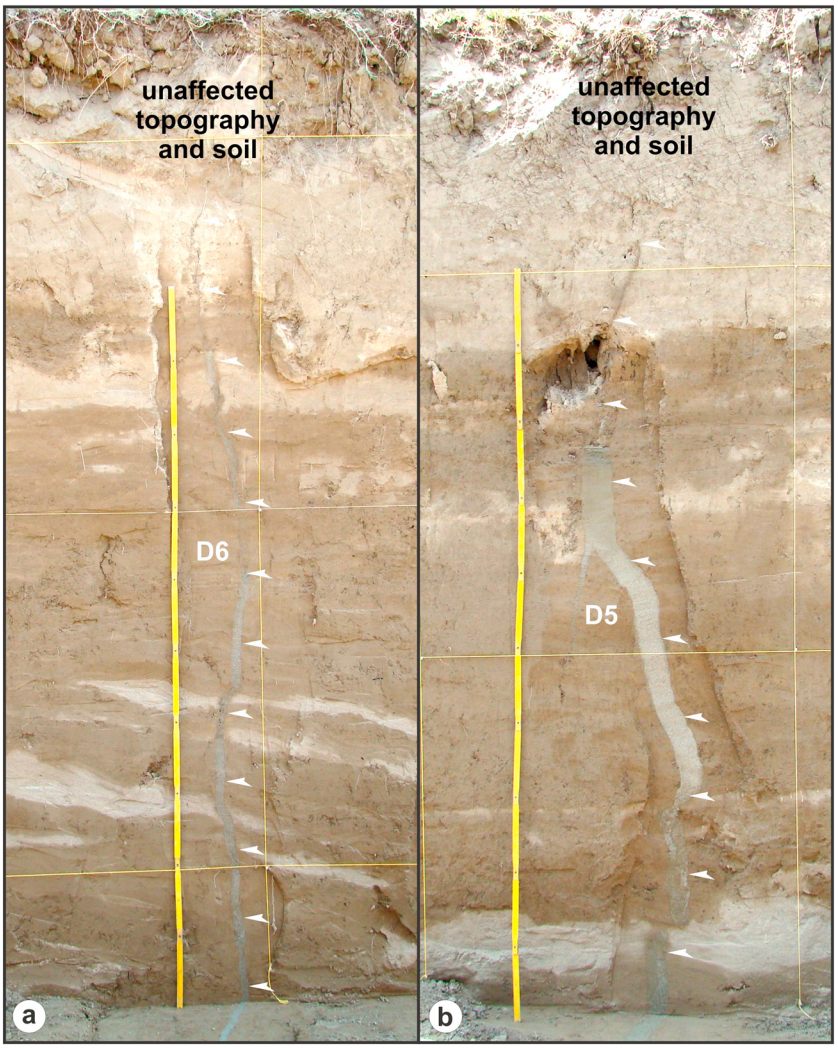

Figure 8. Dikes D6 and D5 characterized by 1–5 and 10 cm, respectively, of sand infilling (i.e., opening), which abruptly disappears at ~1 m below the surface. In the southwestern wall of the trench, both ground ruptures F3 and F4 are represented by submillimetric faint fractures. In plan view, F3 (Figure 4a) clearly tapers SSWward.

(either opening or shear) shows sharp lateral variations. The general setting of the fractures was at high angle, up to subvertical. Fractures F1, F3, and F4 were associated with an almost pure opening, with maximum displacement of a few millimeters.

Fracture F2 was characterized by a normal dip-slip kinematics (western block down) with 20 cm of throw and 5 cm of heave (Figures 5a and 5b). Both pretrenching field observation and trench log of this fracture document the rapid lateral variations of the amount of shearing, which completely disappeared southward (compare the topographic displacement in Figures 5a and 5c).

The detailed trench logging allowed the recognition of a number of dikes (labeled D# in Figure 5) crossing the diverse stratigraphic bodies. They were almost perpendicular to the trench walls and dipping at high angle (70°–90°), both westward and eastward. Although geometrically complex, dikes usually present sharp borders in section view and vary in thickness from less than a millimeter up to 10–12 cm (for example, Figures 6, 7, and 8). In some cases, a small portion of their thickness is likely associated with lateral "excavation" of the fracture walls, more than with a purely kinematic process (i.e., opening). This is suggested by the local mismatch among the fracture walls, since any significant strike-slip component (i.e., out-of-plane relative movement in section view) can be disregarded from field observations. This erosional process possibly occurred during high-pressure injection phases of the water-sand mixture.

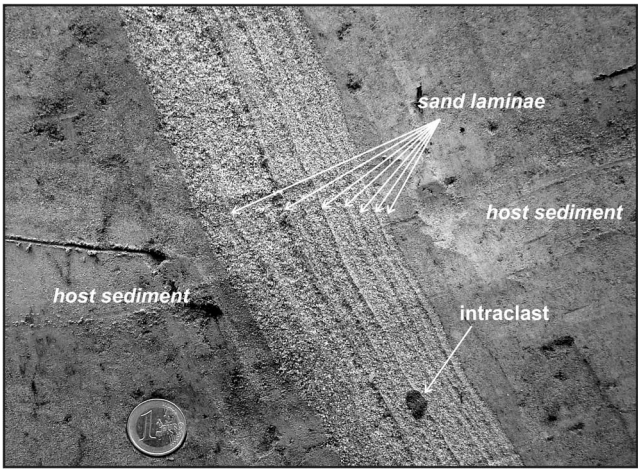

Figure 9. Dike-parallel lamination (vertical section of dike D3 at 4.9 m depth). Single sand layers are graded and separated by thin finer grained laminae. Layering is accentuated by differential erosion. See Figure 5c for location.

Several textural features document the nature of the dike infillings as due to mixed sand and water injected from below (deeper levels) and not to the gravitation infilling from above. Indeed, injection locally occurred by high-velocity flows (Figure 9). The occurrence of such high energy flows is further confirmed by the presence of muddy "intraclasts" in the dike sand, coming from lower sedimentary units (Figure 10).

The presence of multiple bands and laminae, sometimes associated with marked changes in the grain size of the sand (Figures 6, 9, and 10), clearly documents that dikes formed as a consequence of multiple injection events; the subsequent injection events are not necessarily far between them in time, that is to say they could have occurred within seconds or minutes. This could be correlated to several overpressure pulses, typically generated in a shallow (semi)confined aquifer during the seismic shaking of a major earthquake.

Only during the second excavation phase, it was possible to reach the source layer of the dikes infilling, or at least its upper part. At the base of the trench (at 7.0–7.5 m from the surface), medium-to-coarse sand was logged (Figure 11). The same material was also drilled down to a depth of 10.5 m below ground level, during the auxiliary borehole operations (Figure 5a). This sand body belongs to the lower portion of the FCU (see section 2.1). Systematic granulometry and composition analyses confirm that both the grain size distribution and mineralogy of this unit perfectly match those of the trench dikes, while they markedly differ from those characterizing the deeper sands that belong to the upper Pleistocene PAPU deposits [*Fontana et al.*, 2015]. Due to the stratigraphic setting and hydrogeological framework, the source layer represents a semiconfined aquifer, which is characterized by a high degree of liquefaction susceptibility, according to the summer 2012 piezometric level [*Papathanassiou et al.*, 2012]. It is worth noting that the sedimentary interface separating the overlying levee body (deposit "6" in Figure 5) and the underlying medium-to-coarse sands of the source layer (deposit "7" in Figure 5) is intensely deformed (Figure 11). This volume shows clear evidences of a high degree of mobilization in a fluid state (i.e., during a liquefaction process), mixing up the originally tabular (at least at this scale) layers and generating a manifest convolution pattern.

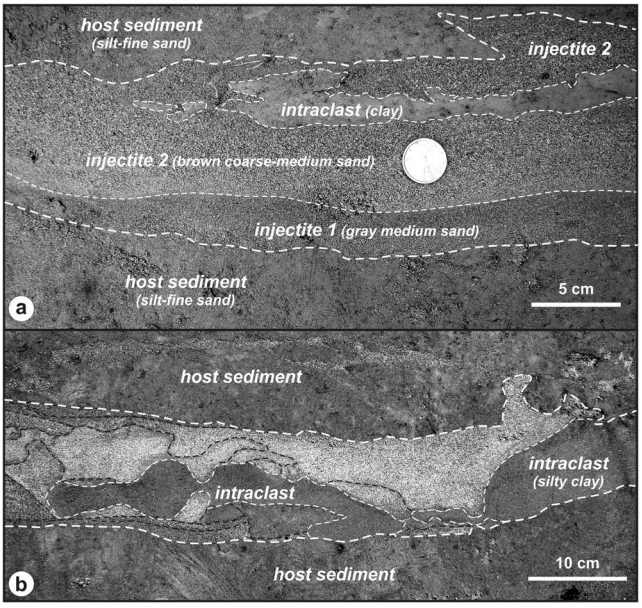

Figure 10. Examples of clay intraclasts within the sandy dikes. Horizontal sections of dike D3 at (a) 4.3 m depth, after the first excavation stage, and (b) at 5.1 m depth, during the second excavation stage.

Other deformational features are represented by "load structures" affecting several 2–10 cm thick sandy layers of the levee body (circles in Figure 5) [*Caputo et al.*, 2012]. The primary depositional geometry of the sand layers was roughly tabular, at the mesoscale. The highly irregular interfaces observed in the trench's

Figure 11. Medium-to-coarse sand unit outcropping at the base of the trench (7.0–7.5 m from surface), which represents the source layer of the dikes infilling, as confirmed by granulometric and compositional analyses [*Fontana et al*., 2015]. Note the mixing up of the sands (*sd*) with clays (*cl*) and clay-silts (*cl-st*) due to a high mobilization, during the liquefaction process.

walls are therefore likely the result from deformation event(s), taking place while the sands were in a temporary viscous state. In this phase, the different density and rheological behavior of sands and clayey silts caused the incipient mixing phenomenon [*Owen*, 2003; *Montenat et al*., 2007]. This observation further confirms that the investigated sedimentary units were involved in a significant liquefaction process.

4. Discussion

This section focuses on the crucial issue of whether the complex deformation structures observed in the trench were induced only by the 2012 seismic events or also previous earthquake(s). In order to answer this question, we discuss all available chronological constraints, both structural and stratigraphic ones.

4.1. Structural Chronological Constraints

Two major apparent anomalies concern the timing of dike formation. First, in spite of the wide, long, and continuous ground ruptures affecting the top of the abandoned levee (Figure 4a), the huge amounts of water-sand mixture outpoured in the surroundings (Figures 4c–4f) and although fracture F2 was associated with a throw of 16 cm and a heave of about 5 cm (i.e., opening), only a very limited amount of ejected material was recorded at the surface within the trench perimeter (yellow dashed line in Figure 4a) following the 20 May main shock. It should be also noted that sand infilling of the corresponding dike D3 was visible in the trench wall up to about 60 cm from the topographic surface (Figures 5 and 7) and, as above mentioned, several textural features within the dikes suggest the occurrence of overpressure pulses. Accordingly, it would be bizarre that an overpressured water-sand mixture had the sufficient energy, first, to create a 10 cm thick dike up to a very shallow level (~ 60 cm from the surface) and, secondly, to generate a macroscopic lateral spreading movement (Figure 4a) but without outpouring at the surface a corresponding important amount of sand.

Secondly, dike D7 is 0.5–5 cm thick and is associated with 15 cm of shear displacement (Figure 12); however, no ground ruptures have been observed at the surface following the 2012 earthquake nor fractures were affecting the trench walls (Figures 5a and 5b). It would be again unrealistic to assume that such an important lateral spreading would have generated 15 cm of sliding affecting most of the palaeolevee body, say 6–8 m thick, without involving the uppermost 60–80 cm of it (Figure 12).

The dikes D2, D3, D5, and D8 are also associated with evident shear displacements of the crossed sedimentary layers (Figure 5c). These features form altogether a graben-like structure (Figure 13), with the two major antithetic sliding surfaces joining at about 6 m depth. By summing up the contribution of the single displacements, it is possible to estimate an overall horizontal lengthening of the levee body of about 20 cm. At the topographic surface no such amount of heave has been however observed (Figure 4a), only the dike D3 and possibly D5 can be correlated with some confidence to fractures F2 and F5, respectively (Figures 5c and 13).

Also other dikes observed in the trench seem uncorrelated to the 2012 fractures. For example, dike D5 (Figure 8b) documents an opening of about 10 cm along its entire length, but it abruptly disappears at ~1 m below the surface. Dike D6 (1–5 cm thick; Figure 8a) similarly disappears at about 1 m depth.

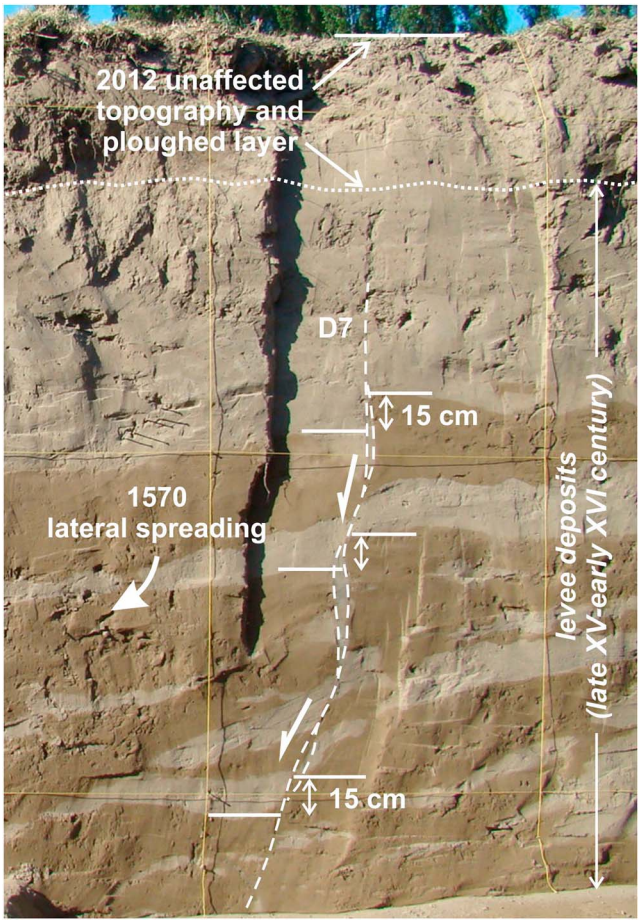

Figure 12. Macroscopic lateral spreading event (15 cm of throw) associated with dike D7, clearly not correlated with any displacement of the plowed layer (uppermost 60 cm) and of the topographic surface (modified from *Caputo et al*. [2012]).

In conclusion, from the observation of dike D3 versus fracture F2 (Figure 7) it is clear that sliding (viz. lateral spreading) and diking are not coeval. In this case, it is obvious that D3 is older than the 2012 event. Similarly, dike D7, associated with macroscopic lateral spreading (15 cm of throw; Figure 12), could not have formed during the 2012 earthquake and must be older, since the topographic surface was not affected. The graben structure, too, provides important chronological constraints. Although some of the dikes, like D3, and possibly D5, have been used as weakness zones during the 20 May 2012 earthquake, for accommodating the shear displacement associated with the ground rupture F2, and possibly F5 (Figures 4 and 5c), the kinematic misfit between the two types of structures (2012 fractures and dikes) indicates that dikes are older than fractures. A further evidence of an older formation of the dikes comes from the structures D5 and D6 (Figure 8) clearly sealed by the uppermost layers of fluvial deposits and obviously by the plowed layer. Based on the depositional framework (sections 2.1 and 3.2), these levee deposits sedimented during the late phases of the Reno channel evolution in the seventeenth and eighteenth centuries.

A final and crucial proof that the liquefaction phenomena documented at the trench site are not associated with the 2012 shaking is represented by the several "load structures" affecting the levee deposits and observed between 1.5 and 2.5 m depth along the internal slope (circles in Figure 5). However, in May 2012 the piezometric level was much lower (~5–5.5 m depth) [*Papathanassiou et al*., 2012], and hence, these deposits were under dry conditions (Figure 14a). Therefore, no liquefaction process and/or plastic behavior could have occurred in these deposits. In contrast, up to the eighteenth century, when this reach of the Reno River was still active, the higher piezometric level (Figure 14b) guaranteed favorable conditions for similar load structures to form.

4.2. Stratigraphic Chronological Constraints

Important chronological constraints can be also obtained by analyzing the stratigraphic setting. Calibrated ^{14}C data (Table 1), together with historical written documentation, allow the definition of an accurate chronological framework of the area stratigraphy. For example, in core 3 (Figure 14a) the PAPU deposits have been dated 19.9 ka B.P. and the middle-lower portion of the interfluvial clay unit (HWU) at 4.9–5.1 ka B.P. [*Cibin and Segadelli*, 2009]. Moreover, in two boreholes drilled few hundred meters away from the trench site (cores 1 and 2; Figure 3), the top level of the same argillaceous unit (HWU) and the base of the overlying fluvial sand body have been independently dated at 1450–1481 A.D. [*Calabrese et al*., 2012] and 1420–1530 A.D. (present work), respectively (Table 1 and Figure 14). This chronological constraint is confirmed by a second shallower sample from core 1 and a wood fragment collected in the palaeoseismological trench providing calibrated ^{14}C ages of 1470–1516 and 1465–1645, respectively (Table 1 and Figure 14). The brick fragment finding

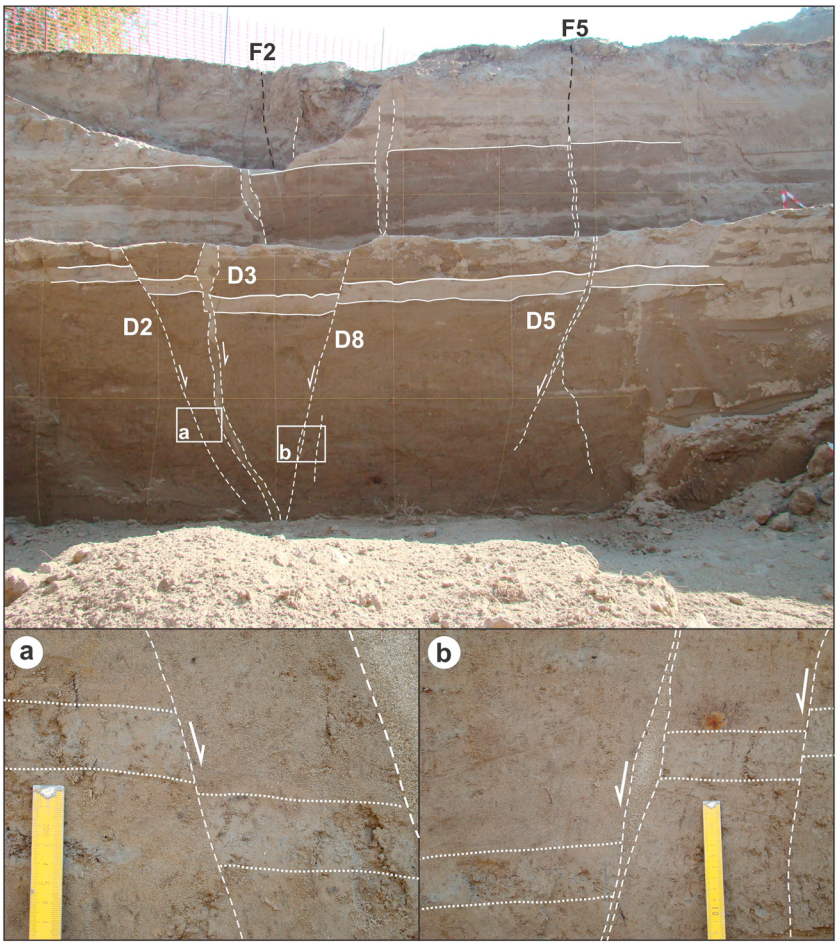

Figure 13. The dike system observed in the southwestern wall of the trench, forming a graben structure (see Figure 5c). The sum of the heaves and openings associated with the dikes largely exceeds that measured at the surface following the 2012 earthquake; similarly, the throws observed at depth in the trench have no equivalent structures at the surface (i.e., ground ruptures).

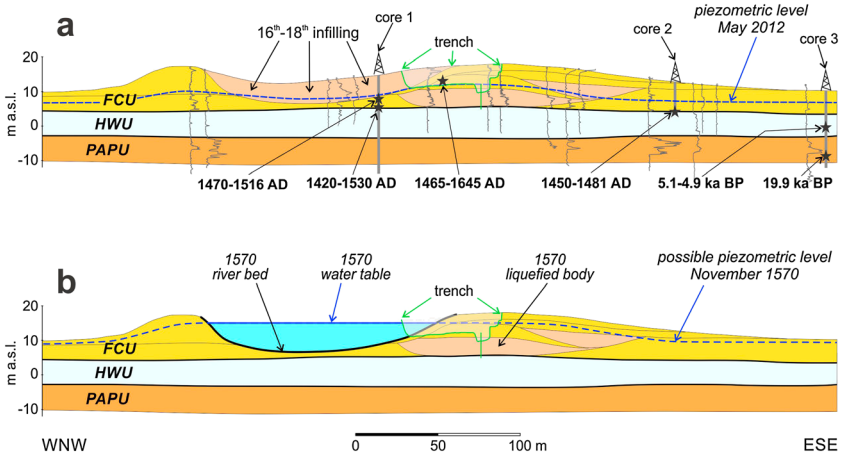

Figure 14. Stratigraphic model across the abandoned reach of the Reno River, reconstructed on the basis of several penetrometric tests, shallow cores, and the trench logs. The sedimentary bodies belonging to the *FCU* (see section 2.1) were mainly deposited during the late fifteenth-early sixteenth centuries. The May 2012 piezometric level is from *Papathanassiou et al.* [2012], while that of November 1570 is inferred from a likely water table level of the river, during a period of autumn high water level. See Table 1 for more details on radiochronological ages. See Figure 3 for cores locations. The stratigraphic section exposed in the trench is also indicated.

Table 1. Available Calibrated ^{14}C Ages From the Investigated Area[a]

Sample Site and Code	Stratigraphic Unit	Latitude (N)	Longitude (E)	Depth (m)	Calibrated ^{14}C Age	Reference
Trench (SC1-15) Beta-417575	FCU	44°47′57″	11°24′05″	5.3	1465–1645 A.D. (95.4%)	1
Core 1 (S10-C1) ETH-47160	FCU	44°48′13″	11°24′26″	6.2	1470–1516 A.D. (95.4%)	2
Core 1 (SC1-24/S10) LTL12720	FCU	44°48′13″	11°24′26″	7.8	1420–1530 A.D. (79.6%)	1
Core 2 (S4-C2) ETH-47159	HWU	44°48′09″	11°24′31″	7.4	1450–1481 A.D. (95.4%)	2
Core 3 (203-S6) Beta	HWU	44°47′11″	11°24′07″	13.8	5.1–4.9 ka B.P. (95.4%)	3
Core 3 (203-S6) ENEA	PAPU	44°47′11″	11°24′07″	20.2	19.9 ka B.P.	3

[a]For site location see Figure 3 (cores 1–3) and Figure 5 (for trench sample). Stratigraphic units are described in section 2.1. References: (1) present work; (2) *Calabrese et al.* [2012]; (3) *Cibin and Segadelli* [2009]. B.P. values are referred to 1950.

within the fluvial sands (Figure 5a) also suggests a postmedieval origin of the fluvial sedimentary body. In summary, all these ages clearly constrain the chronology of the FCU, which started forming only during the (mid-)late fifteenth century.

On the other hand, the detailed palaeogeographic and historical reconstruction synthesized in section 2.2 documents that the bulk of the fluvial body at the trench site accumulated between the ending of the fifteenth century and the beginning of the sixteenth century with an impressive aggradation rate in the order of 15–20 cm/a. In fact, since that period the Reno River levee north of Sant'Agostino became a morphologically stable strip of land, where the permanent (viz. not seasonal) road connecting Cento to Ferrara (reaches d, e, and f in Figure 2) was established. This implies that further levee aggradation was a negligible process in the following centuries. Indeed, only the uppermost overbank deposits observed in the trench, say 0.5–1 m deep, were accumulated at this later stage and likely concentrated during the paroxistic flooding years 1731–1735. These youngest deposits are also basically coeval with the rapid infilling process of the channel (partly observed in the trench), which definitely dried up in the fall-winter 1764–1765 [*Fiocca*, 2003].

5. Conclusions

The structural analysis carried out at the trench demonstrates that the shaking caused by the 2012 earthquakes reactivated older coseismic secondary structures (viz. subvertical discontinuities) and that likely none of the observed more or less thick dikes were formed during the 20 May event. Only minor contributions in few cases could be not excluded. Therefore, the causative event for most of the observed seismically induced features must be older than that. The careful inspection of the dikes visible in the trench walls (Figures 7, 8, and 12) also clearly shows that they do not affect the plowed soil, and, more importantly, they are sealed by the uppermost sedimentary layer of the levee body. The latter sediments cannot be younger than the mideighteenth century when this reach of the Reno River definitely dried up. On the other hand, the chronostratigraphic framework (Table 1 and Figure 14) of the affected FCU deposits rule out the whole of the medieval earthquakes as triggering events of the liquefaction phenomena, since the levee body mainly deposited in late fifteenth and early sixteenth centuries times (see sections 2.2 and 4). In summary, the time window for the possible causative event can therefore be restricted at most to less than three centuries (sixteenth tot eighteenth) and we accordingly searched for it in the historical catalogues of the broader region [e.g., *Guidoboni et al.*, 2007; *Locati et al.*, 2011].

Based on the Environmental Seismic Intensity 2007 scale [*Michetti et al.*, 2007] the San Carlo site was classified as VIII [*Papathanassiou et al.*, 2012], which is slightly larger than the VI-VII of the MCS scale [*Galli et al.*, 2012]. This discrepancy is likely due to the two different scales, the former exclusively based on the environmental seismic effects and the latter on the macroseismic ones focusing on damaged buildings and other man-made structures. However, in order to compare the 2012 event with past ones by exploiting the available historical catalogues [e.g., *Guidoboni et al.*, 2007; *Locati et al.*, 2011], only a common scale (i.e., MCS) must be used. Taking into account that the reported intensity in the area of San Carlo-Sant'Agostino during the 20 May earthquake is VI-VII MCS [*Galli et al.*, 2012] and that the threshold intensity to induce liquefaction is commonly assumed at VI MCS [e.g., *Galli*, 2000], we considered only historical events with at least $I_0 \geq$ VI. Based on macroseismic attenuation relationships [e.g., *Grandori et al.*, 1987] and ground motion prediction equations [e.g., *Bindi et al.*, 2011] commonly applied in Italy as well as on empirical relations between magnitude, intensity, and maximum distance for liquefied sites [*Ambraseys*, 1988; *Papadopoulos and Lefkopoulos*, 1993; *Papathanassiou et al.* 2005; *Castilla and Audemard*, 2007],

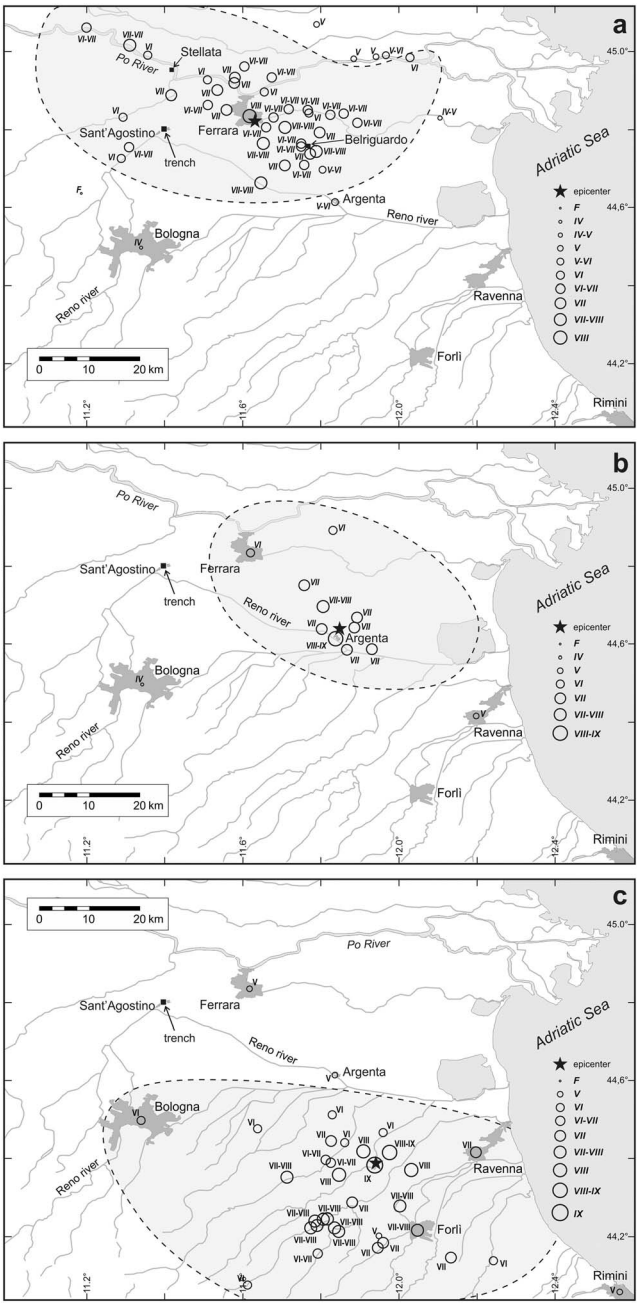

Figure 15. The macroseismic fields of the (a) Ferrara 1570 (17 November), (b) Argenta 1624 (18 March), and (c) Romagna 1688 (11 April) earthquakes. Stars represent the corresponding macroseismic epicenters calculated with the Boxer code [*Gasperini et al.*, 1999]. Maps modified from *Locati et al.* [2011]. The dashed lines are purely indicative of the VI MCS isoseismal curve. All values are in MCS scale.

we excluded the events with an epicentral distance from the trench site greater than 100 km because of the natural decay of the shaking with distance.

In this framework, the only possible candidates are the Ferrara 1570 (17 November), Argenta 1624 (18 March), and Romagna 1688 (11 April) earthquakes(with epicentral intensity of VII-VIII, VII-VIII, and VIII-IX MCS and equivalent magnitude of 5.5, 5.5, and 5.8, respectively) [*Guidoboni et al.*, 2007; *Locati et al.*, 2011]. It should be noted that the 1570 event has been recently re-estimated and a moment magnitude of 5.8 has been proposed [*Sirovich and Pettenati*, 2015].

We therefore analyzed the macroseismic fields of these earthquakes (Figure 15). Although purely indicative, in Figure 15 we tentatively draw the isoseismal curves corresponding to the VI MCS. A careful inspection of the overall intensities distribution associated to both younger events (1624 and 1688) seems not compatible with the occurrence, at the investigated area, of at least an intensity VI MCS, capable of triggering the diffuse and important liquefaction effects observed in the trench. It is clear that even considering the possible occurrence of some local effects, these two earthquakes were too remote from the study site to be able the triggering of palaeoliquefactions. In contrast, in the 1570 macroseismic field, the study site is surrounded by several intensity values of VI, VI-VII, and VII MCS (Figure 15) and it is clearly enclosed in the VI MCS isoseismal curve. It is therefore reasonable that a sufficiently strong shaking affected at that time the area of San Carlo, and we conclude that the secondary geological effects observed in the excavation, like the thick dikes (up to 10 cm), the macroscopic sliding of levee blocks and the load casts, were very likely associated with the Ferrara earthquake of 17 November 1570.

As a matter of fact, the chronicles of this earthquake document the occurrence of environmental effects and sand ejections in the town of Ferrara and in its surroundings [*Galli*, 2000; *Guidoboni et al.*, 2007]. No sufficient historical information and geographic details are available for precisely locating the sites affected by liquefaction [*De Martini et al.*, 2014], but a good empirical estimation is nevertheless available. The distance of San Carlo from the estimated epicenter (18 km) is similar to those of Stellata and Belriguardo (21 and 13 km, respectively; Figure 15a), where severe environmental effects were recorded and it is compatible with those

predicted by several empirical relationships for secondary effects [*Ambraseys*, 1988; *Papadopoulos and Lefkopoulos*, 1993; *Galli*, 2000; *Aydan et al*., 2000; *Papathanassiou et al*., 2005].

It is also worth noting that the 1570 event occurred during a phase of high fluvial water level (Figure 14b), associated to the seasonal period of heavy precipitations. As a consequence, the piezometric level in the levee body was reasonably much higher than the one measured during the summer 2012 (Figure 14a) [*Papathanassiou et al*., 2012]. This peculiar hydrogeological setting, corresponding to a greater pore pressure within the aquifer, certainly favored the occurrence of widespread liquefaction phenomena in the identified source layer (unit 7 in Figure 5) [*Fontana et al*., 2015], the consequent triggering of macroscopic lateral spreading sliding, the opening of fractures, the subsequent injection of an overpressured sand-water mixture, and the formation of thick dikes. These 1570 coseismic structures, and particularly dikes and ground offsets, were then sealed by younger deposits, associated with the latest aggradational phases that occurred on top of the levee body in the early eighteenth century.

During the May 2012 earthquake, some of the buried structures were partially reactivated as weakness zones for "simply" accommodating some sliding induced by lateral spreading phenomena as observed at the trench site and surroundings (Figures 4 and 5). However, the piezometric level during the summer 2012 was probably not adequately high to trigger a diffuse and intense liquefaction process, while no differential loads were acting at the trench site due to the absence of buildings and other heavy infrastructures (Figure 4 a). In contrast, the presence of such overloads in the surroundings of the trench area (Figures 4c–4f) as well as in other densely built areas of San Carlo and Mirabello villages likely induced in the nearby sedimentary successions a sufficiently strong confining pressure and water overpressure to produce the numerous secondary effects and the consequent diffuse damage observed [*Crespellani et al*., 2012; *Carydis et al*., 2012; *Galli et al*., 2012; *Di Manna et al*., 2012; *Tertulliani et al*., 2012; *Dolce and Di Bucci*, 2014]. It should be, however, noted that extensive sand ejection has locally occurred also in other free-field conditions [e.g., *Bertolini and Fioroni*, 2012], though limited to the alluvial plain or to the lower sector of the abandoned levees and never on their top. As a matter of fact, these geological conditions are characterized by a thinner sedimentary cap and a shallower water depth, which are much more prone to liquefaction.

As a final remark, we want to stress how a typical palaeoseismological approach can be also applied in the absence of primary fault ruptures while investigating blind faults and can provide crucial information on past moderate-to-strong earthquakes that affected a region. This has the potential to expand the seismotectonic knowledge and hence contribute to improve future seismic hazard assessment analyses. Although the selection of the trench site is obviously a critical point, which should be based on a systematic search of the most favorable areas prone to liquefaction, it is also undoubt the applicability of this method to other seismogenic areas worldwide.

Acknowledgments

We are grateful to the Municipality of Sant'Agostino and particularly to the Major Fabrizio Toselli and his staff for providing technical, financial, and logistic support and to the owner of the trench site (Giuseppe Fortini) for permitting the large excavation. Many thanks to Grillanda s.r.l. for their crucial technical support during the second phase of the trench works. Thanks to the Servizio Geologico, Sismico e dei Suoli, and Regione Emilia-Romagna (Luca Martelli) for providing the DEM of the San Carlo area (Figure 3) and access to the sedimentary cores drilled near the investigated area (included in Figure 14) and to Giovanni Bertolini ARPA-RER for providing the airphotos of the trench site (Figure 4). Radiocarbon age from the trench site has been performed by Beta Analytics Inc. (sample number Beta-417575). ArcGIS software has been used for Figures 1, 2, and 3. Suggestions by L. Piccardi, two anonymous reviewers, and the Editors (P. Vannucchi and C. Faccenna) contributed to improve the manuscript.

References

Abu Zeid, N., S. Bignardi, R. Caputo, G. Santarato, and M. Stefani (2012), Electrical Resistivity Tomography investigation on coseismic liquefaction and fracturing at San Carlo, Ferrara Province, Italy, *Ann. Geophys.*, *55*(4), 713–716, doi:10.4401/ag-6149.

Adams, J. (1982), Deformed lake sediments record prehistoric earthquakes during the degiaciation of the Canadian Shield (abstr.), *Eos Trans. AGU*, *63*(18), 436.

Ambraseys, N. (1988), Engineering seismology, *J. Earthq. Eng. Struct. Dyn.*, *17*, 1–105.

Amick, D., and R. Gelinas (1991), The search for evidence of large prehistoric earthquakes along the Atlantic seaboard, *Science*, *251*(4994), 655–658.

Amick, D., R. Gelinas, G. Maurath, R. Cannon, D. Moore, E. Billington, and H. Kemppinen (1990), Paleoliquefaction features along the Atlantic seaboard, *U.S. Nucl. Regul. Commission Rep.*, NUREG CR-5613, 146 pp.

Audemard, F. A., and F. de Santis (1991), Survey of liquefaction structures induced by recent moderate earthquakes, *Bull. Int. Assoc. Eng. Geol.*, *44*, 5–16.

Aydan O., R. Ulusay, H. Kumsar, and E. Tuncay (2000), Site investigation and engineering evaluation of the Duzce-Bolu earthquake of November 12, 01999, Turkish Earthquake Foundation, Instanbul, Rep. No. TDV/DR 09-51, 307 pp.

Bartolini, C., R. Caputo, and M. Pieri (1996), Pliocene-Quaternary sedimentation in the Northern Apennine Foredeep and related denudation, *Geol. Magazine*, *133*(3), 255–273, Cambridge.

Bertolini, G., and C. Fioroni (2012), Aerial inventory of surficial geological effects induced by the recent Emilia earthquake (Italy): Preliminary report, *Ann. Geophys.*, *55*(4), 705–711, doi:10.4401/ag-6113.

Bigi, G., G. Bonardini, R. Catalano, D. Cosentino, F. Lentini, M. Parotto R. Sartori, P. Scandone, and E. Turco (1992), Structural model of Italy, 1:500,000, Consiglio Nazionale delle Ricerche, Rome.

Bignami, C., et al. (2012), Coseismic deformation pattern of the Emilia 2012 seismic sequence imaged by Radarsat-1 interferometry, *Ann. Geophys.*, *55*(4), 788–795, doi:10.4401/ag-6157.

Bindi, D., F. Pacor, L. Luzi, R. Puglia, M. Massa, G. Ameri, and R. Paolucci (2011), Ground motion prediction equations derived from the Italian strong motion database, *Bull. Earthquake Eng.*, *9*, 1899–1930, doi:10.1007/s10158-011-9313-z.

Boccaletti, M., M. Bonini, G. Corti, P. Gasperini, L. Martelli, L. Piccardi, C. Tanini, and G. Vannucci (2004), Seismotectonic map of the Emilia-Romagna Region, 1:250000, Regione Emilia-Romagna – CNR.

Bondesan, M. (1989), Evoluzione geomorfologica e idrografica della pianura ferrarese, Terre ed acqua, Corbo Editore, 14–20.

Bondesan, M. (2001), L'evoluzione idrografia e ambientale della pianura ferrarese negli ultimi 3000 anni, in *Storia di Ferrara*, *Territorio e Preistoria*, vol. 1, edited by M. Bondesan and A. Broglio, pp. 227–263, Corbo Ed. Ferrara, Ferrara, Italy.

Bondesan, M., R. Ferri, and M. Stefani (1995), Rapporti fra lo sviluppo urbano di Ferrara e l'evoluzione idrografia, sedimentaria e geomorfologica del territorio, in *Ferrara nel Medioevo; topografia storica e urbana*, edited by A. M. Visser Travagli, pp. 27–42, Ed. Grafis, Bologna, Italy.

Bonini, L., G. Toscani, and S. Seno (2014), Three-dimensional segmentation and different rupture behavior during the 2012 Emilia seismic sequence (Northern Italy), *Tectonophysics*, *630*, 33–42, doi:10.1016/j.tecto.2014.05.006.

Burrato, P., F. Ciucci, and G. Valensise (2003), An inventory of river anomalies in the Po Plain, Northern Italy: Evidence for active blind thrust faulting, *Ann. Geophys.*, *46*(5), 865–882.

Burrato P., P. Vannoli, U. Fracassi, R. Basili, and G. Valensise (2012), Is blind faulting truly invisible? Tectonic-controlled drainage evolution in the epicentral area of the May 2012, Emilia-Romagna earthquake sequence (northern Italy), *Ann. Geophys.*, *55*(4), 525–531, doi:10.4401/ag-6182.

Calabrese, L., L. Martelli, and P. Severi (2012), Stratigrafia dell'area interessata dai fenomeni di liquefazione durante il terremoto dell'Emilia (maggio 2012). 31° Conv. Naz. GNGTS, Potenza, November 20–22, 2012, *Atti*, *2*, 119–126.

Caputo, R. (2005), Ground effects of large morphogenic earthquakes, *J. Geodyn.*, *40*(2–3), 113–118, doi:10.1016/j.jog.2005.07.001.

Caputo, R., and B. Helly (2008), The use of distinct disciplines to investigate past earthquakes, *Tectonophysics*, *453*(1–4), 7–19.

Caputo, R., and G. Papathanassiou (2012), Ground failure and liquefaction phenomena triggered by the 20 May, 2012 Emilia-Romagna (Northern Italy) earthquake: Case study of Sant'Agostino–San Carlo–Mirabello zone, *Nat. Haz. Earth System Sciences*, *12*(11), 3177–3180, doi:10.5194/nhess-12-3177-2012.

Caputo, R., K. Iordanidou, L. Minarelli, G. Papathanassiou, M. E. Poli, D. Rapti-Caputo, S. Sboras, M. Stefani, and A. Zanferrari (2012), Geological evidence of pre-2012 seismic events, Emilia-Romagna, Italy, *Ann. Geophys.*, *55*(4), 743–749, doi:10.4401/ag-6148.

Caputo, R., A. Pellegrinelli, C. Bignami, A. Bondesan, A. Mantovani, S. Stramondo, and P. Russo (2015), High-precision levelling, DInSAR and geomorphological effects in the Emilia 2012 epicentral area, *Geomorphology*, *235*, 106–117, doi:10.1016/j.geomorph.2015.02.002.

Carannante, S., A. Argnani, M. Massa, E. D'Alema, S. Lovati, M. Moretti, M. Cattaneo, and P. Augliera (2015), The May 20 (M_w 6.1) and 29 (M_w 6.0), 2012, Emilia (Po Plain, northern Italy) earthquakes: New seismotectonic implications from subsurface geology and high-quality hypocenter location, *Tectonophysics*, *655*, 107–123, doi:10.1016/j.tecto.2015.05.015.

Carydis, P., C. Castiglioni, E. Lekkas, I. Kostaki, N. Lebesis, and A. Drei (2012), The Emilia Romagna, May 2012 earthquake sequence: The influence of the vertical earthquake component and related geoscientific and engineering aspects, *Ing. Sismica*, *29*(2–3), 31–58.

Castaldini, D. (1989), Evoluzione della rete idrografica centropadana in epoca protostorica e storica. Convegno Nazionale di Studi, Cento May 8–9, 1987, *Atti Acc. Sci. Ferrara*, (Suppl. 64), pp. 113–134.

Castaldini, D., and S. Raimondi (1985), Geomorfologia dell'area di Pianura Padana compresa fra Cento, Finale Emilia e S. Agostino, *Atti Soc. Nat. Mat Modena*, *116*, 147–176.

Castellarin, A., L. Cantelli, A. M. Fesce, J. Mercier, V. Picotti, G. A. Pini, G. Prosser, and L. Selli (1992), Alpine compressional tectonics in the Southern Alps. Relations with the N-Apennines, *Ann. Tectonicae*, *6*, 62–94.

Castello, B., G. Selvaggi, C. Chiarabba, and A. Amato (2006), CSI Catalogo della sismicità italiana 1981–2002, version 1.1. INGV-CNT, Roma. [Available at: http://www.ingv.it/CSI/.]

Castiglioni, G., et al. (1999), Geomorphological map of the Po Plain, Italy, at a scale of 1:250.000, *Earth Surf. Processes Landforms*, *24*, 1115–1120.

Castilla, R. A., and F. A. Audemard (2007), Sand blows as a potential tool for magnitude estimation of pre-instrumental earthquakes, *J. Seismol.*, *11*, 473–487, doi:10.1007/s10950-007-9065-z.

Cazzola, F., P. Luciani, and G. Capuzzo (1995), E la terra emerse dalle acque : Le fasi storiche della grande bonificazione ferrarese: Dallo scolo naturale al sollevamento meccanico, Ferrara, Cazzola F., Luciani P. and Capuzzo G. (1995): E la terra emerse dalle acque : Le fasi storiche della grande bonificazione ferrarese: Dallo scolo naturale al sollevamento meccanico. Ferrara, Consorzio di Bonifica Primo Circondario, Polesine di Ferrara, 103 pp.

Cesca, S., T. Braun, F. Maccaferri, L. Passarelli, E. Rivalta, and T. Dahm (2013), Source modelling of the M5–6 Emilia-Romagna, Italy, earthquakes (2012 May 20–29), *Geophys. J. Int.*, *193*, 1658–1672, doi:10.1093/gji/ggt069.

Chini, M., et al. (2015), Coseismic liquefaction phenomenon analysis by COSMO-SkyMed: 2012 Emilia (Italy) earthquake, *Int. J. Appl. Earth Observ. Geoinfo.*, *39*, 1–14, doi:10.1016/j.jag.2015.02.008.

Cibin, U., and S. Segadelli (Eds.) (2009), Note Illustrative della Carta Geologia d'Italia alla scala 1:50.000, Foglio 203, Poggio Renatico. Servizio Geologico d'Italia, 104 pp.

Cremaschi, M., and G. Gasperi (1989), La "alluvione" alto-medievale di Mutina (Modena) in rapporto alle variazioni ambientali oloceniche, *Mem. Soc. Geol. It.*, *42*, 179–190.

Cremonini, S. (1988), Specificità dell'Alto Ferrarese nella problematica evolutiva dell'antica idrografia padana inferiore, in *Bondeno ed il suo territorio dalle origini al Rinascimento*, pp. 17–24, Grafis Ed., Bologna, Italy.

Cremonini, S. (1991), Una "finestra geomorfica" d'età classica nella pianura bolognese. Inquadramento analitico del gruppo morfologico del Reno antico, in "*Romanità della Pianura. L'ipotesi archeologica a S. Pietro in Casale come coscienza storica per una nuova gestione del territorio*, pp. 243–301, Atti Giornate di Studio, 7/8 Aprile 1990, Bologna.

Crespellani, T., J. Facciorusso, A. Ghinelli, C. Madiai, S. Renzi, and G. Vannucchi (2012), Rapporto preliminare dui diffusi fenomeni di liquefazione verificatisi durante il terremoto in Pianura Padana emiliana del maggio 2012, Univ. Firenze, 33 pp.

Crone A. J., M. Giardino, and E. S. Schweig (1995), Paleoseismic studies of the of the Bootheel lineament, southeastern Missouri, and the Crittenden County fault zone, northeastern Arkansas, New Madrid seismic zone, central United States. *Miscellaneous Field Studies*, map MF-2279, U.S. Geol. Surv.

Database of Individual Seismogenic Sources (DISS) Working Group (2015), Database of Individual Seismogenic Sources (DISS), Version 3.2.0: A compilation of potential sources for earthquakes larger than M 5.5 in Italy and surrounding areas, Istituto Nazionale di Geofisica e Vulcanologia, doi:10.6092/INGV.IT-DISS3.2.0.

De Martini, P. M., F. R. Cinti, L. Cucci, A. Smedile, S. Pinzi, C. A. Brunori, and F. Molisso (2012), Sand volcanoes induced by the April 6th 2009 M_w 6.3 L'Aquila earthquake: A case study from the Fossa area, *Ital. J. Geosci.*, *131*(3), 410–422, doi:10.3301/IJG.2012.14.

De Martini, P. M., et al. (2014), Correlation, using chronological datings, between liquefaction events in the area of the May–June 2012 Emilia seismic sequence and known earthquakes of the past. In: Argnani A. (Ed.), DPC-INGV Seismological Programme 2012–2013, *Final Rep.*, D17.b2, 154–205,

Devoti, R., A. Esposito, G. Pietrantonio, A. R. Pisani, and F. Riguzzi (2011), Evidence of large scale deformation patterns from GPS data in the Italian subduction boundary, *Earth Planet. Sci. Lett.*, *311*, 230–241, doi:10.1016/j.epsl.2011.09.034.

Dewey, J. F., M. L. Helman, E. Turco, D. H. W. Hutton, and S. D. Knott (1989), *Kinematics of the western Mediterranean*, in *Alpine Tectonics*, edited by M. P. Coward, D. Dietrich, and R. G. Park, *Geol. Soc. London Spec. Publ.*, 45, 265–283.

Di Cocco, I. (2009), L'applicazione della banca dati archeologica alla cartografia geologica di pianura, *Note Illustrative della Carta Geologia d'Italia alla scala 1:50.000, Foglio 202, San Giovanni in Persiceto* edited by F. C. Molinari and M. Pizziolo, 104 pp.

Di Domenica, A., L. Bonini, F. Calamita, G. Toscani, C. Galuppo, and S. Seno (2014), Analogue modeling of positive inversion tectonics along differently oriented prethrusting normal faults: An application to the Central-Northern Apennines of Italy, *Geol. Soc. Am. Bull.*, *126*(7–8), 943, doi:10.1130/B31001.1.

Di Manna, P., et al. (2012), Ground effects induced by the 2012 seismic sequence in Emilia: Implications for seismic hazard assessment in the Po Plain, *Ann. Geophys.*, *55*(4), 697–703.

Doglioni, C. (1993), Some remarks on the origin of foredeeps, *Tectonophysics*, *228*, 1–20.

Dolce, M., and D. Di Bucci (2014), National Civil Protection Organization and technical activities in the 2012 Emilia earthquakes (Italy), *Bull. Earthq. Eng.*, *12*, 2231–2253, doi:10.1007/s10518-014-9597-x.

Emergeo Working Group (2013), Liquefaction phenomena associated with the Emilia earthquake sequence of May–June 2012 (Northern Italy), *Nat. Haz. Earth Syst. Sci.*, *13*, 935–947.

Enzel, Y., R. Bookman, D. Sharon, H. Gvirtsman, U. Dayan, B. Ziv, and M. Stein (2003), Late Holocene climates of the Near East deduced from Dead Sea level variations and modern regional winter rainfall, *Quat. Res.*, *60*, 263–273, doi:10.1016/j.yqres.2003.07.011.

Fiocca C. (2003), Vicende idrauliche del Basso Po nella corrispondenza di Gian Andrea Barotti e Romualdo Bertaglia. Atti del Convegno Cultura nell'Età delle Legazioni, Ferrara, 1–20.

Fontana, D., S. Lugli, S. Marchetti Dori, R. Caputo, and M. Stefani (2015), Sedimentology and composition of sands injected during the seismic crisis of May 2012 (Emilia, Italy): Clues for source layer identification and liquefaction regime, *Sediment. Geol.*, *325*, 158–167, doi:10.1016/j.sedgeo.2015.06.004.

Franceschini, A. (1983), Una storia di acque, in edited by R. Sitti, *Vigarano, Storia/Attualità*, pp. 21–50, Arstudio C, Ferrara, Italy.

Frizzi, A. (1848), *Memorie per la storia di Ferrara*, Abram Servadia Editore, Ferrara, Italy.

Gabrielli R. (1999), Prime analisi mensiocronologiche dei laterizi della città di Bologna. Archeologia dell'Architettura, vol. IV, pp. 149–158, "All'Insegna del Giglio", Florence, Italy.

Galli, P. (2000), New empirical relationships between magnitude and distance for liquefaction, *Tectonophysics*, *324*, 169–187.

Galli, P., S. Castenetto, and E. Peronace (2012), The MCS macroseismic survey of the 2012 Emilia earthquakes, *Ann. Geophys.*, *55*(4), 663–672, doi:10.4401/ag-6163.

Gasperini, P., F. Bernardini, G. Valensise, and E. Boschi (1999), Defining seismogenic sources from historical earthquakes felt reports, *Bull. Seism. Soc. Am.*, *89*(1), 94–110.

Ghielmi, M., M. Minervini, C. Nini, S. Rogledi, M. Rossi, and A. Vignolo (2010), Sedimentary and tectonic evolution in the eastern Po-Plain and northern Adriatic Sea area from Messinian to Middle Pleistocene (Italy), *Rend. Fis. Acc. Lincei*, *21*(Suppl. 1), S131–S166, doi:10.1007/s12210-010-0101-5.

Govoni, A., et al. (2014), The 2012 Emilia seismic sequence (Northern Italy): Imaging the thrust fault system by accurate aftershock location, *Tectonophysics*, *622*, 44–55, doi:10.1016/j.tecto.2014.02.013.

Grandori, G., F. Perotti, and A. Tagliani (1987), On the attenuation of macroseismic intensity with epicentral distance, in edited by A. S. Cakmak, *Ground Motion and Engineering Seismology*, *Developments in Geotechnnical Engineering*, vol. 44, edited by A. S. Cakmak, pp. 581–594, Elsevier, Amsterdam.

Guidoboni, E., G. Ferrari, D. Mariotti, A. Comastri, G. Tarabusi, and G. Valensise (2007), CFTI4Med, catalogue of strong earthquakes in Italy (461 B.C.-1997) and the Mediterranean area (760 B.C.-1500), INGV-SGA. [Available at http://storing.ingv.it/cfti4med/.]

Hempton, M. R., and J. F. Dewey (1983), Earthquake-induced deformational structures in young lacustrine sediments, East Anatolia Fault, southeast Turkey, *Tectonophysics*, *98*, T7–T14.

Istituto superiore per la protezione e la ricerca ambientale (ISPRA) (2009), *Carta Geologica d'Italia, scala 1:50.000, Foglio 203 Poggio Renatico*, edited by U. Cibin and S. Segadelli, Regione Emilia Romagna-ISPRA, Rome.

Istituto superiore per la protezione e la ricerca ambientale (ISPRA) (2012), Geological effects induced by the seismic sequence started on May 20, 2012, *in Emilia (Mw=5.9) Prelim. Rep. Open File Rep., Open file report*. Servizo Geologico d'Italia, 10 pp.

Livio, F. A., et al. (2009), Active fault-related folding in the epicentral area of the December 25, 1222 (Io = IX MCS) Brescia earthquake (Northern Italy): Seismotectonic implications, *Tectonophysics*, *476*, 320–335, doi:10.1016/j.tecto.2009.03.019.

Locati, M., R. Camassi, and M. Stucchi (Eds.) (2011), *DBMI11, la versione 2011 del Database Macrosismico Italiano*, Milano, Bologna, Italy, doi:10.6092/INGV.IT-DBMI11.

Maesano, F. E., and C. D'Ambrogi (2015), Coupling sedimentation and tectonic control: Pleistocene evolution of the central Po Basin, *Ital. J. Geosci.*, *134*, doi:10.3301/IJG.2015.17.

Maesano, F. E., C. D'Ambrogi, P. Burrato, and G. Toscani (2015), Slip-rates of blind thrusts in slow deforming areas: Examples fromthe Po Plain (Italy), *Tectonophysics*, *643*, 8–25, doi:10.1016/j.tecto.2014.12.007.

Mantovani, E., D. Albarello, C. Tamburelli, D. Babbucci, and M. Viti (1997), Plate convergence, crustal delamination, extrusion tectonics and minimization of shortening work as main controlling factors of the recent Mediterranena deformation pattern, *Ann. Geofis.*, *40*(3), 611–643.

Mantovani, E., M. Viti, D. Babbucci, C. Tamburelli, and D. Albarello (2001), Back arc extension: Which driving mechanism?, *J. Virtual Explorer*, *3*, 17–44.

Mariotti, G., and C. Doglioni (2000), The dip of the foreland monocline in the Alps and Apennines, *Earth Planet. Sci. Lett.*, *181*, 191–202.

Martelli, L., A. Benini, M. T. De Nardo, and P. Severi (2009), Note Illustrative della Carta Geologica d'Italia, Foglio 220, Casalecchio di Reno. Regione Emilia Romagna e APAT, scala 1:50,000. Servizio Geologico, Sismico e dei Suoli, Regione Emilia Romagna, System Cart S.r.l., Roma, 124 pp.

Massa, M., P. Augugliera, G. Franceschina, S. Lovati, and M. Zupo (2012), The July 17, 2011, M_L 4.7, Po Plain (northern Italy) earthquake: Strong-motion observations from the RAIS network, *Ann. Geophys.*, *55*(2), 309–321, doi:10.4401/ag-5389.

Mele, F., B. Castello, A. Marchetti, C. Marcocci, and R. Moro (2007), ISIDe, Italian Seismological Instrumental and parametric DatabasE: una pagina web per interrogare il Bollettino Sismico Italiano (a web page to query the Italian Seismic Bulletin), 26° Convegno Nazionale GNGTS. [Availabe at http://www2.ogs.trieste.it/gngts/gngts/convegniprecedenti/2007/riassunti/tema-1/1-sess-1/11-mele.pdf.]

Michetti, A. M., et al. (2007), Intensity scale ESI 2007, in *Memorie Descrittive Carta Geologica d'Italia*, vol. LXXIV, edited by L. Guerrieri, and E. Vittori, APAT, Servizio Geologico d'Italia - Dipartimento Difesa del Suolo, 53 pp., Roma, Italy.

Molinari, F. C., G. Boldrini, P. Severi, G. Duroni, D. Rapti-Caputo, and G. Martinelli (2007), Risorse idriche sotterranee della Provincia di Ferrara, Regione Emilia Romagna, DB MAP Ed. (Florence), pp. 61.

Montenat, C., P. Barrier, P. O. d'Estevou, and C. Hibsch (2007), Seismites: An attempt at critical analysis and classification, *Sedim. Geol.*, *196*, 5–30, doi:10.1016/j.sedgeo.2006.08.004.
Mörner, N.-A. (2003), *Paleoseismicity of Sweden: A Novel Paradigm*, *320 pp.*, JOFO Grafiska AB, Stockholm.
Munson, P. J., C. A. Munson, and N. K. Bleuer (1994), Late Pleistocene and Holocene earthquake-induced liquefaction in the Wabash Valley of southern Indiana. In: M.L. Jacobson (Comp.), National Earthquake Hazards Reduction Program, summaries of technical reports, vol. XXXV, *U.S. Geol. Surv. Open File Rep. 94-176*, 553–557.
Munson, P. J., C. A. Munson, N. K. Bleuer, and M. D. Labitzke (1992), Distribution and dating of prehistoric liquefaction in the Wabash Valley of the Central US, *Seismol. Res. Lett.*, *63*(3), 337–342.
Ninfo, A., D. Zizioli, C. Meisina, D. Castaldini, F. Zucca, L. Luzi, and M. De Amicis (2012), The survey and mapping of sand-boil landforms related to the Emilia 2012 earthquakes: preliminary results, *Ann. Geophys.*, *55*(4), 735–742.
Obermeier, S. F. (1989), The New Madrid earthquakes: An engineering-geologic interpretation of relict liquefaction features, *U.S. Geol. Surv. Open File Rep.*, 1336 B, 114 pp.
Obermeier, S. F. (1996), Using liquefaction-induced and other soft-sediment features for paleoseismic analysis, in *Paleoseismology*, edited by J. P. McCalpin, pp. 331–396, Academic Press, San Diego, Calif.
Obermeier, S. F., R. E. Weems, and R. B. Jacobson (1987), Earthquake-induced liquefaction features in the coastal South Carolina region. *U.S. Geol. Surv. Open File Rep. 87–504,* 20 pp.
Owen, G. (2003), Load structures: gravity-driven sediment mobilization in the shallow subsurface, *Geol. Soc. London Spec. Publ.*, *216*, 21–34.
Papadopoulos, G. A., and G. Lefkopoulos (1993), Magnitude-distance relations for liquefaction in soil from earthquakes, *Bull. Seismol. Soc. Am.*, *83*(3), 925–938.
Papathanassiou, G., S. Pavlides, B. Christaras, and K. Pitilakis (2005), Liquefaction case histories and empirical relations of earthquake magnitude versus distance from the broader Aegean region, *J. Geodyn.*, *40*, 257–278.
Papathanassiou, G., R. Caputo, and D. Rapti-Caputo (2012), Liquefaction-induced ground effects triggered by the 20th May, 2012 Emilia-Romagna (Northern Italy) earthquake, *Ann. Geophys.*, *55*(4), 735–742, doi:10.4401/ag-6147.
Papathanassiou, G., A. Mantovani, G. Tarabusi, D. Rapti, and R. Caputo (2015), Assessment of liquefaction potential for two liquefaction prone area considering the May 20, 2012 Emilia (Italy) earthquake, *Eng. Geol.*, *189*, 1–16, doi:10.1016/j.enggeo.2015.02.002.
Peterson, C. D., M. Hansen, and D. Jones (1991), Widespread evidence of paleoliquefaction in late-Pleistocene marine terraces from the Oregon and Washington margins of the Cascadia subduction zone (abstr.), *Eos Trans. AGU*, *72*(44), 313.
Pezzo, G., et al. (2013), Coseismic deformation and source modeling of the May 2012 Emilia (Northern Italy) earthquakes, *Seismol. Res. Lett.*, *84*(4), 645–655, doi:10.1785/0220120171.
Pieri, M., and G. Groppi (1981), Subsurface geological structure of the Po Plain, Italy, Consiglio Nazionale delle Ricerche, Progetto finalizzato Geodinamica, sottoprogetto Modello Strutturale, pubbl. N° 414, Roma, 13 pp.
Pizzi, A., and V. Scisciani (2012), The May 2012 Emilia (Italy) earthquakes: Preliminary interpretations on the seismogenic source and the origin of the coseismic ground effects, *Ann. Geophys.*, *55*(4), 751–757, doi:10.4401/ag-6171.
Pondrelli, S., S. Salimbeni, G. Ekström, A. Morelli, P. Gasperini, and G. Vannucci (2006), The Italian CMT dataset from 1977 to the present, *Phys. Earth Planet. Inter.*, *159*(3–4), 286–303, doi:10.1016/j.pepi.2006.07.008.
Pondrelli, S., S. Salimbeni, P. Perfetti, and P. Danecek (2012), Quick regional centroid moment tensor solutions for the Emilia 2012 (northern Italy) seismic sequence, *Ann. Geophys.*, *55*(4), 615–621, doi:10.4401/ag-6146.
Rinaldi R. (2005), Dalla via Emilia al Po. Il disegno del territorio e i segni del popolamento (secc. VIII-XIV). Biblioteca di Storia agraria Medievale Club, Bologna, 1–79.
Ringrose, P. S. (1989), Paleoseismic (?) liquefaction event in late Quaternary lake sediments at Glen Roy, Scotland, *Terra Nova*, *1*(1), 57–62.
Rodríguez-Pascua, M. A., P. S. Silva, R. Pérez-Lòpez, J. L. Giner-Robles, F. Martín-Gonzàlez, and B. Del Moral (2015), Polygenetic sand volcanoes: On the features of liquefaction processes generated by a single event (2012 Emilia Romagna 5.9 M_w earthquake, Italy), *Quat. Int.*, *357*, 329–335, doi:10.1016/j.quaint.2014.09.020.
Robertson, A. H. F., and M. Grasso (1995), Overview of the Late Tertiary-Recent tectonic and palaeo-environmental development of the Mediterranean region, *Terra Nova*, *7*(2), 114–127.
Rogledi, S. (2010), Assetto strutturale delle unità alpine nella pianura tra il lago d'Iseo e il Garda. Rischio sismico nella pianura tra il lago d'Iseo e il Garda Presented at the Workshop "Rischio sismico nella Pianura Padana", Brescia 24 November 2010. [Available at http://cesia.ing.unibs.it/index.php/it/eventi/giornate-di-studio/119.]
Rovida, A., R. Camassi, P. Gasperini, and M. Stucchi (Eds) (2011), CPTI11, la versione 2011 del Catalogo Parametrico dei Terremoti Italiani. Istituto Nazionale di Geofisica e Vulcanologia, Milano, Bologna, doi:10.6092/INGV.IT-CPTI11.
Russ, D. P. (1979), Late Holocene faulting and earthquake recurrence in the Reelfoot Lake area, northwestern Tennessee, *Geol. Soc. Am. Bull.*, *90*, 1013–1018.
Salvi, S., C. Tolomei, J. P. Merryman Boncori, G. Pezzo, S. Atzori, A. Antonioli, E. Trasatti, R. Giuliani, S. Zoffoli, and A. Coletta (2012), Activation of the SIGRIS monitoring system for ground deformation mapping during the Emilia 2012 seismic sequence, using COSMO-SkyMed InSAR data, *Ann. Geophys.*, *55*(4), 797–802, doi:10.4401/ag-6181.
Saucier, R. T. (1991), Geoarchaeological evidence of strong prehistoric earthquakes in the New Madrid (Missouri) seismic zone, *Geology*, *19*(4), 296–298.
Scrocca, D., E. Carminati, C. Doglioni, and D. Marcantoni (2007), Slab retreat and active shortening along the Central-Northern Apennines, in *Thrust Belts and Foreland Basins: From Fold Kinematics to Hydrocarbon Systems*, edited by O. Lacombe et al., pp. 471–487, Springer, Berlin.
Seilacher, A. (1969), Fault-graded beds interpreted as seismites, *Sedimentology*, *13*(1–2), 155–159, doi:10.1111/j.1365-3091.1969.tb01125.x.
Serpelloni, E., S. Danesi, C. Tolomei, A. Cavaliere, A. Gualandi, L. Anderlini, and S. Salimbeni (2015), New geodetic and seismological constraints on active shortening across the pedeapennines and pedeAlpine regions, in *Project S1 "Base Knowledge Improvement for Assessing the Seismogenic Potential of Italy", Final Rep.*, edited by A. Argnani, S. Danesi and S. Castenetto, pp. 58–82.
Sirovich, L., and F. Pettenati (2015), Source inversion of the 1570 Ferrara earthquake and definitive diversion of the Po River (Italy), *J. Geophys. Res. Solid Earth*, *120*, 5747–5763, doi:10.1002/2015JB012340.
Stefani, M. (2006), Il contesto paleogeografico e sedimentologico-stratigrafico della necropoli romana del Verginese, in *Mors inmatura. I Fadieni e il loro sepolcreto*, edited by F. Berti, pp. 16–41, Edizioni "All" Insegna del Giglio, Florence, Italy.
Stefani, M., and S. Vincenzi (2005), The interplay of eustasy, climate and human activity in the late Quaternary depositional evolution and sedimentary architecture of the Po Delta system, *Mar. Geol.*, *222–223*, 19–48, doi:10.1016/j.margeo.2005.06.029.
Sukhija, B. S., M. N. Rao, D. V. Reddy, P. Nagabhushama, S. Hussain, R. K. Chadha, and H. K. Gupta (1999), Paleoliquefaction evidence and periodicity of large prehistoric earthquakes in Shillong Plateau, India, *Earth Planet. Sci. Letts.*, *167*, 269–282.
Tertulliani, A., et al. (2012), The Emilia 2012 sequence: A macroseismic survey, *Ann. Geophys.*, *55*(4), 679–687, doi:10.4401/ag-6140.

Tizzani, P., et al. (2013), New insights into the 2012 Emilia (Italy) seismic sequence through advanced numerical modeling of ground deformation InSAR measurements, *Geophys. Res. Lett.*, *40*, 1–7, doi:10.1002/GRL.50290.

Tuttle, M. P. (1994), The liquefaction method for assessing paleoseismicity, *U.S. Nucl. Regul. Commission Rep.*, NUREG/CR-6258, 38 pp.

Tuttle, M. P. (2001), The use of liquefaction features in paleoseismology: Lessons learned in the New Madrid seismic zone, central United States, *J. Seismol.*, *5*, 361–380.

Tuttle, M. P., and E. C. Schweig (1995), Archeological and pedological evidence for large prehistoric earthquakes in the New Madrid seismic zone, central United States, *Geology*, *23*(3), 253–256.

Vannoli, P., P. Burrato, and G. Valensise (2015), The seismotectonics of the Po Plain (Northern Italy): Tectonic diversity in a blind faulting domain, *Pure Appl. Geophys.*, *172*, 1105–1142, doi:10.1007/s00024-014-0873-0.

Wesnousky, S. G., and L. M. Leffler (1992), The repeat time of the 1811 and 1812 New Madrid earthquakes: A geological perspective, *Bull. Seismol. Soc. Am.*, *82*(4), 1756–1784.

Zoetemeijer, R., W. Sassi, F. Roure, and S. Cloetingh (1992), Stratigraphic and kinematic modeling of thrust evolution, northern Apennines, Italy, *Geology*, *20*, 1035–1038.